Available online at www.sciencedirect.com
ScienceDirect
Journal of Sound and Vibration 304 (2007) 124–153
JOURNAL OF SOUND AND VIBRATION
www.elsevier.com/locate/jsvi

Free vibration analysis of axially loaded cracked Timoshenko beam structures using the dynamic stiffness method

E. Viola[a,*], P. Ricci[a], M.H. Aliabadi[b]

[a]Distart Department, University of Bologna, Viale Risorgimento 2, Bologna 40136, Italy
[b]Department of Aeronautics, Imperial College, Prince Consort Road, South Kensington, London, UK

Received 24 November 2006; received in revised form 7 February 2007; accepted 7 February 2007

Abstract

In this article, the purpose is to investigate the changes in the magnitude of natural frequencies and modal response introduced by the presence of a crack on an axially loaded uniform Timoshenko beam using a particular member theory. A new and convenient procedure based on the coupling of dynamic stiffness matrix and line-spring element is introduced to model the cracked beam. The application of the theory is demonstrated by two illustrative examples of bending–torsion coupled beams with different end conditions, for which the influence of axial force, shear deformation and rotatory inertia on the natural frequencies is studied. Moreover, a parametric study to investigate the effect of the crack on the modal characteristics of the beam is conducted.

1. Introduction

The present paper addresses coupled bending–torsional vibration of axially loaded cracked beams within the context of the dynamic stiffness matrix (DSM) method of analysing structures. Such coupled vibration is particularly important for the aerospace industry because of its aeroelastic applications.

Helicopter, propeller and also compressor and turbine blades of a high aspect ratio, all qualify (at least for their first few vibration modes) as axially loaded beams which usually have non-coincident elastic and inertial axes [1]. Applications of such elements also include aeroelastic calculations for which coupled bending–torsional frequencies and modes are essential requirements [2–4]. Moreover, as with the finite element method, the DSM method can be extended to cover the vibration analysis of structures consisting of many elements. Some plane or space frames can be represented within reasonable accuracy as an assemblage of axially loaded coupled beams connected together. Naturally, it is very important to take into account the coupling effects in vibration and response calculations of this type of structures. The effect of an important parameter, namely the axial force, which is usually negligible or non-existent for some structures such as aircraft wings (but not so for helicopter, turbine or propeller blades), has also to be taken into account.

*Corresponding author. Tel.: +39 051 2093510; fax: +39 051 2093495.
E-mail address: erasmo.viola@mail.ing.unibo.it (E. Viola).

0022-460X/$ - see front matter © 2007 Elsevier Ltd. All rights reserved.
doi:10.1016/j.jsv.2007.02.013

Nomenclature

a	crack length
A	area of the cross-section
b	breadth flange of the T-section
d	width of the T-section
E	Young's modulus
E_s	shear centre of the T-section
G	shear modulus
G_s	mass centre of the T-section
h	height of the cross-section
$\bar{h}$	deflection of the cross-section
$H(y)$	amplitudes of the sinusoidally varying vertical displacement
I	moment of inertia of the section
I_G	polar mass moment of inertia per unit length through the centroid
I_α	polar mass moment of inertia per unit length about the Y-axis
k	section shape factor
$\mathbf{k}_f$	stiffness matrix of the line spring
$\mathbf{K}$	dynamic stiffness matrix
K_{I}, K_{II}, K_{III}	stress intensity factor for modes I, II and III
L	length of the beam
m	mass per unit length
M	bending moment
p^2	term corresponding to the effect of the axial force
P	axial force
r^2	term corresponding to the effect of the rotatory inertia
s^2	term corresponding to the effect of the shear deformation
S	shear force
t	time
T	torque
x_α	distance of separation between the elastic axis and the mass axis
θ	flexural rotations of the cross-section
$\Theta(y)$	amplitudes of the sinusoidally varying bending rotation
λ_{mm}, λ_{ss}, λ_{tt}	compliances for bending moment, shear force and torsion
ν	Poisson's coefficient
ξ	dimensionless length of the beam element
ρ	density
ψ	torsional rotations of the cross-section
$\Psi(y)$	amplitudes of the sinusoidally varying torsional rotation
ω	circular frequency

Using traditional methods that are based on the derivation of differential equations and application of boundary conditions, the Bernoulli–Euler beam theory has been available in the literature since the 18th century [5]. The above theory has been studied by a number of investigators, whereas it was not until around 1941 that the corresponding DSM was developed by Kolousek [6,7] who later included it in a textbook [8]. Exact analytical expressions for displacement functions and element stiffness matrices can thus be established. Likewise Timoshenko [9,10] solved the vibration problem of a Bernoulli–Euler beam with the effects of shear deformation and rotatory inertia included (i.e. the Timoshenko beam) in the earlier part of last century and then, after several years, Cheng [11] and Wang and Kinsman [12] developed the DSM of such beams. Later the DSM of an axially loaded Timoshenko beam was developed by Howson and Williams [13] and by Cheng and Tseng [14].

The derivation of the equations of motion for the coupled bending–torsion vibrations of axially loaded beams, has been studied by different authors (see e.g., [15–17]) and numerous approaches for calculating the free vibrational natural frequencies and mode shapes have been proposed. The stiffness expressions include the effects of shear deformation and rotatory inertia, which are significant for beams having large cross-sectional dimensions in comparison to their lengths and also when higher modes are important.

The stiffness matrix, in this method, is obtained by solving the governing differential equation directly, and hence all assumptions, being within the limits of the differential equations only, are less severe. For this reason, results obtained using a DSM are often justifiably called "exact" [16].

The present paper develops the explicit DSM of a cracked axially loaded, bending–torsion coupled beam with the effects of the rotatory inertia and the shear deformation included.

There are only few applications about the dynamic stiffness method to investigate the vibration characteristics of cracked beams undergoing coupled bending and torsional displacements. A survey by the authors shows that there is a gap in the literature in this respect. The central purpose of this paper is to fill this

gap and extend the elegance of the dynamic stiffness method to the case of a uniform axially loaded Timoshenko cracked beam. Another aim of this work is to present some accurate data, which might be useful to other researchers when validating their results. To this end coupled bending–torsional frequencies and modal shapes of cracked T-beams are presented in this paper for clamped–free and hinged–hinged boundary conditions by excluding and including the effect of axial force, shear deformation and rotatory inertia.

It should be noted that, unlike the finite element method in which the mass and stiffness matrices of a structural element are obtained separately, the dynamic stiffness method involves only one frequency-dependent matrix called the DSM. The matrix in discussion is obtained from the exact analytical solution of the governing differential equations of motion of the element undergoing free natural vibration.

Once the initial assumptions on the displacement field have been made, the resulting differential equations are solved in an exact form and no further approximation is introduced. Thus, the resulting element matrix features exactly the mass and stiffness properties of the element. It is worth noting that the finite element method uses approximate shape functions of the structural element.

The dynamic stiffness matrices in a structure can be assembled in a manner similar to that of the finite element method, except that only one overall DSM is obtained (instead of separate mass and stiffness matrices) for the complete structure. It should be noted that when dealing with free vibration problems, the dynamic stiffness method leads to a transcendental eigenvalue problem, whereas the finite element method usually leads to a linear eigenvalue problem. It is also significant that the accuracy of results using the finite element method depends on the numbers of elements used whereas the dynamic stiffness method has no such limitation because it accounts for an infinite number of natural frequencies of a vibrating structure and thus the results are independent of the number of elements used in the analysis. For instance, one single dynamic stiffness structural element can be used to determine any number of natural frequencies of the element to any desired accuracy. This is, of course, impossible in traditional finite element method.

Of particular interest in this work, is to study the coupled bending–torsional vibration behaviour of cracked beams within the context of the DSM method of analysing structures. The authors present a modelling technique based on the combination of the line-spring element stiffness matrix, used to model an open crack and dynamic stiffness matrices. The entire structure is first divided into several substructures, depending on the number of cracks of the beam. The dynamic stiffness matrices of the substructures become the basic matrices for assembling the global DSM for the original structure. The order of the system eigenvalue equation is equal to the number of physical coordinates between the substructures and the line-spring stiffness matrix. The number of modes predicted by the model is not limited by the number of degrees of freedom used in the model. If only one crack is present in the beam, the structure is divided into two substructures, on the left and on the right of the crack, and the global DSM can be obtained by applying the standard procedure of the finite element method. After introducing the boundary conditions at the ends of the beam, one finally obtains the dynamic equilibrium equation. It is seen that the model established by the proposed method, which has only a few degrees of freedom, can predict all eigenmodes of the cracked structure within a large frequency range.

The results are comparable to the FEM results in which a much larger number of elements are necessarily used.

In order to illustrate the procedure and to show the simplicity and efficiency of the method, illustrative examples are given for a bending–torsion coupled cantilever and hinged–hinged beams with a T cross-section. The influence of axial force, shear deformation and rotatory inertia on the natural frequencies and modal shapes is demonstrated.

2. Theoretical considerations

A straight uniform beam element of length L and of T-cross-section is shown in Fig. 1, with the mass axis and the elastic axis (i.e. the loci of the mass centre and the shear centre of the cross-section) being separated by a distance x_α. In the right-handed coordinate system of Fig. 1, the elastic axis, which is assumed to coincide with the y-axis, is permitted flexural translation $\bar{h}(y, t)$ in the z-direction and torsional rotation $\psi(y, t)$ about the y-axis, where y and t denote distance from the origin and time, respectively. A constant compressive axial

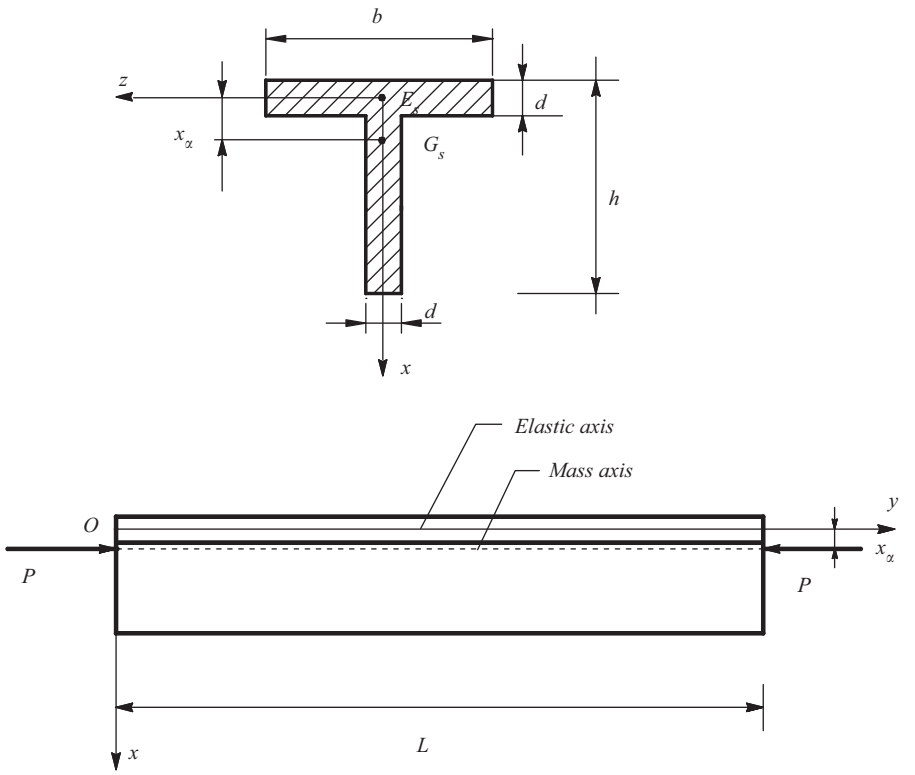

Fig. 1. Coordinate system for a coupled bending–torsional axially loaded Timoshenko uncracked beam with T cross-section.

load P is assumed to act through the centroid (mass centre) of the cross-section. P can be positive or negative, so that tension is included.

The governing partial differential equations of motion for the coupled bending–torsional free natural vibration of the axially loaded Timoshenko beam shown in Fig. 1 are given by [18]

$$EI\theta'' + kAG(\bar{h}' - \theta) - \rho I\ddot{\theta} = 0, \tag{1}$$

$$kAG(\bar{h}'' - \theta') - P(\bar{h}'' - x_\alpha\psi'') - m(\ddot{\bar{h}} - x_\alpha\ddot{\psi}) = 0, \tag{2}$$

$$GJ\psi'' - P\{(I_\alpha/m)\psi'' - x_\alpha\bar{h}''\} - I_\alpha\ddot{\psi} + mx_\alpha\ddot{\bar{h}} = 0, \tag{3}$$

where E is the Young's modulus, G is the shear modulus and ρ is the density of the material, EI, GJ and kAG are, respectively, the bending, torsional and shear rigidities of the beam, I is the second moment of area of the beam cross-section about the x-axis, k is the section shape factor, A is the cross-section area, $m = \rho A$ is the mass per unit length, I_α is the polar mass moment of inertia per unit length about the y-axis (i.e. an axis through the shear centre), θ is the angle of rotation in radians of the cross-section due to the bending alone (so that the total slope $\bar{h}'$ equals the sum of slope due to bending and due to shear deformation) and primes and dots denote differentiation with respect to position y and time t, respectively.

Eqs. (1)–(3) together with appropriate end conditions completely define the coupled bending–torsional free vibration of an axially loaded uniform Timoshenko beam. If a sinusoidal variation of $\bar{h}$, θ and ψ with circular frequency ω, is assumed, then

$$\begin{aligned} \bar{h}(y,t) &= H(y)\sin\omega t, \\ \theta(y,t) &= \Theta(y)\sin\omega t, \\ \psi(y,t) &= \Psi(y)\sin\omega t, \end{aligned} \tag{4}$$

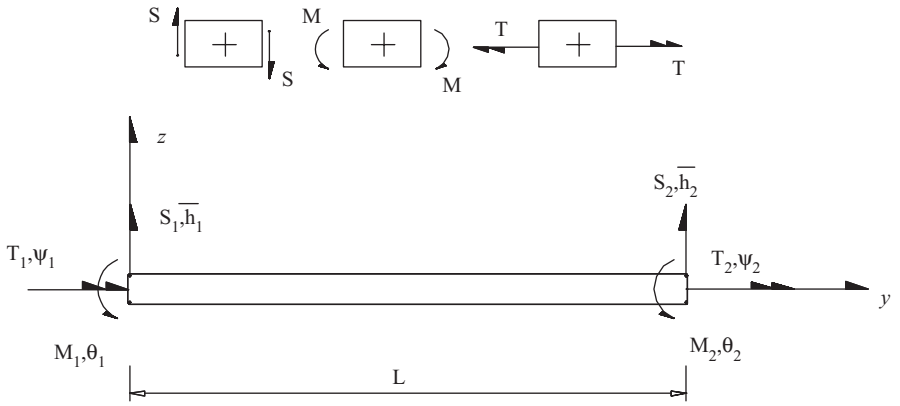

Fig. 2. Sign convention for positive transverse (shear) force S, bending moment M and torque T end conditions for forces and displacement of the beam element.

where $H(y)$, $\Theta(y)$ and $\Psi(y)$ are the amplitudes of the sinusoidally varying vertical displacement, bending rotation and twist, respectively.

Substituting Eqs. (4) into Eqs. (1)–(3), the amplitude of $\bar{h}$, θ and ψ are obtained in terms of a set of arbitrary constants.

By extensive algebraic manipulation, the solution for the bending displacement $H(\xi)$, bending rotation $\Theta(\xi)$ and torsional rotation $\Psi(\xi)$ are obtained from the following:

$$H(\xi) = A_1 \cosh \alpha\xi + A_2 \sinh \alpha\xi + A_3 \cos \beta\xi + A_4 \sin \beta\xi + A_5 \cos \gamma\xi + A_6 \sin \gamma\xi, \tag{5}$$

$$\Theta(\xi) = B_1 \sinh \alpha\xi + B_2 \cosh \alpha\xi + B_3 \sin \beta\xi + B_4 \cos \beta\xi + B_5 \sin \gamma\xi + B_6 \cos \gamma\xi, \tag{6}$$

$$\Psi(\xi) = C_1 \cosh \alpha\xi + C_2 \sinh \alpha\xi + C_3 \cos \beta\xi + C_4 \sin \beta\xi + C_5 \cos \gamma\xi + C_6 \sin \gamma\xi, \tag{7}$$

where A_1-A_6, B_1-B_6 and C_1-C_6 are the three different sets of constants, $\xi = y/L$ and α, β, γ are constants reported in Refs. [17,18].

Following the sign convention of Fig. 2, the expressions for the bending moment $M(\xi)$, the transverse force $S(\xi)$ and the torque $T(\xi)$ are obtained from Eqs. (5) to (7), after some simplification, as

$$M(\xi) = -(EI/L)\frac{\mathrm{d}\Theta}{\mathrm{d}\xi}, \tag{8}$$

$$S(\xi) = -\left(EI/L^3\right)\left[L\frac{\mathrm{d}^2\Theta}{\mathrm{d}\xi^2} + p^2\left(\frac{\mathrm{d}H}{\mathrm{d}\xi} - x_\alpha\frac{\mathrm{d}\Psi}{\mathrm{d}\xi}\right) + b^2r^2\Theta L\right], \tag{9}$$

$$T(\xi) = (GJ/L)\left[(1 - p^2a^2/b^2)\frac{\mathrm{d}\Psi}{\mathrm{d}\xi} + \{p^2a^2(1-c^2)/(x_\alpha b^2)\}\right]\frac{\mathrm{d}H}{\mathrm{d}\xi} \tag{10}$$

with

$$\begin{aligned} &a^2 = I_\alpha\omega^2L^2/GJ, \quad b^2 = m\omega^2L^4/EI, \quad c^2 = 1 - mx_\alpha^2/I_\alpha = I_G/I_\alpha,\\ &p^2 = PL^2/EI, \quad r^2 = I/AL^2, \quad s^2 = EI/kAGL^2, \end{aligned} \tag{11}$$

where I_G is the polar mass moment of inertia per unit length about an axis through the centroid and s^2, which represents the shear deformation, is related to the definition of the constants α, β, γ.

The end conditions for displacements and forces of the beam element (see Fig. 2) are, respectively, displacements:

$$\begin{aligned} &\text{at end } 1 \rightarrow (\xi = 0): H = H_1,\ \Theta = \Theta_1,\ \Psi = \Psi_1,\\ &\text{at end } 2 \rightarrow (\xi = 1): H = H_2,\ \Theta = \Theta_2,\ \Psi = \Psi_2 \end{aligned} \tag{12}$$

forces

$$\begin{aligned} &\text{at end } 1 \rightarrow (\xi = 0): S = S_1,\ M = M_1,\ T = -T_1,\\ &\text{at end } 2 \rightarrow (\xi = 1): S = -S_2,\ M = -M_2,\ T = T_2. \end{aligned} \tag{13}$$

The DSM which relates the amplitudes of the sinusoidally varying forces to the corresponding displacement amplitudes can now be derived from the following system:

$$\begin{bmatrix} S_1 \\ M_1 \\ T_1 \\ S_2 \\ M_2 \\ T_2 \end{bmatrix} = \begin{bmatrix} K_{11} & K_{12} & K_{13} & K_{14} & K_{15} & K_{16} \\ & K_{22} & K_{23} & K_{24} & K_{25} & K_{26} \\ & & K_{33} & K_{34} & K_{35} & K_{36} \\ & & & K_{44} & K_{45} & K_{46} \\ & \text{Symmetric} & & & K_{55} & K_{56} \\ & & & & & K_{66} \end{bmatrix} \begin{bmatrix} H_1 \\ \Theta_1 \\ \Psi_1 \\ H_2 \\ \Theta_2 \\ \Psi_2 \end{bmatrix}, \tag{14}$$

which can be represented in a compact form as

$$\mathbf{F} = \mathbf{K}\,\mathbf{U}, \tag{15}$$

where $\mathbf{K}$ is the required stiffness matrix.

The terms of the required stiffness matrix, see Eq. (15), can be found from

$$\begin{aligned} &K_{11} = K_{44} = (EI/L^3)(\Phi_1/\Delta), && K_{22} = K_{55} = (EI/L)(\Phi_7/\Delta),\\ &K_{12} = -K_{45} = (EI/L^2)(\Phi_2/\Delta), && K_{23} = -K_{56} = (x_\alpha EI/L^2)(\Phi_8/\Delta),\\ &K_{13} = K_{46} = (x_\alpha EI/L^3)(\Phi_3/\Delta), && K_{25} = (EI/L)(\Phi_9/\Delta),\\ &K_{14} = (EI/L^3)(\Phi_4/\Delta), && K_{26} = -K_{35} = (x_\alpha EI/L^2)(\Phi_{10}/\Delta),\\ &K_{15} = -K_{24} = (EI/L^2)(\Phi_5/\Delta), && K_{33} = K_{66} = (GJ/L)(\Phi_{11}/\Delta),\\ &K_{16} = K_{34} = (x_\alpha EI/L^3)(\Phi_6/\Delta), && K_{36} = (GJ/L)(\Phi_{12}/\Delta), \end{aligned} \tag{16}$$

where Φ_i ($i = 1,\ldots,12$) and Δ are defined in Ref. [18].

Eqs. (16) give all the terms of the DSM $\mathbf{K}$ of Eqs. (14) and (15). Note that none of these terms are zero but (see Eqs. (16)) that the terms K_{13}, K_{16}, K_{23}, K_{26}, K_{34}, K_{35}, K_{46}, and K_{56} reduce to zero when $x_\alpha = 0$, i.e. when the shear centre and the mass centre of the beam cross-section are coincident.

The DSM is then the one for an axially loaded Timoshenko beam, i.e. an axially loaded Bernoulli–Euler beam with effects of shear deformation and rotatory inertia included, because $x_\alpha = 0$ can be substituted in the derived expressions without causing any overflow or underflow. In computing the DSM, the terms corresponding to the effects of axial force, shear deformation and rotatory inertia (p^2, s^2 and r^2, respectively) can optionally be made zero, with x_α non-zero, to give stiffnesses identical to those given, respectively, by the coupled bending–torsional theories for a Timoshenko beam, an axially loaded Bernoulli–Euler beam and a Bernoulli–Euler beam with non-coincident mass and shear centre. Additionally, when $x_\alpha = 0$, $p^2 = 0$, $s^2 = 0$ and $r^2 = 0$, the computed DSM of Eqs. (15) gives the same stiffness as those of a Bernoulli–Euler beam.

3. Line-spring stiffness matrix and global dynamic stiffness matrix

In order to study the behaviour of a cracked structure, a suitable model of the cracked section is required. Hereinafter, the cracked section is represented as an elastic hinge [19] with spring constants simulating flexural, shear and torsional deformations (see Fig. 3).

The DSM $\mathbf{K}_g$ of a cracked beam of length L (Fig. 4) can be split into a stiffness matrix with three different parts: the stiffness of two uncracked beams of length L_1 and L_2 combined with a "local" stiffness part composed by "springs" which represent the crack (Fig. 4). These springs have an infinite stiffness when the crack is closed and a finite stiffness when the crack is open. If we want to extract the local stiffness due to the

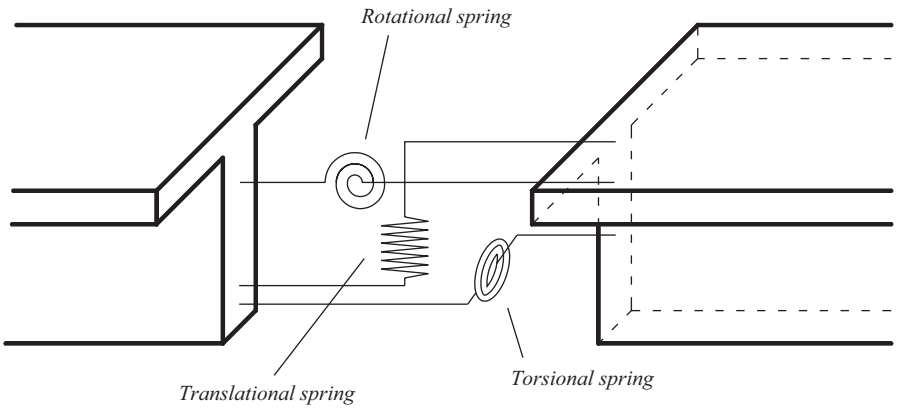

Fig. 3. Model of the cracked beam section with the three springs generating a line spring.

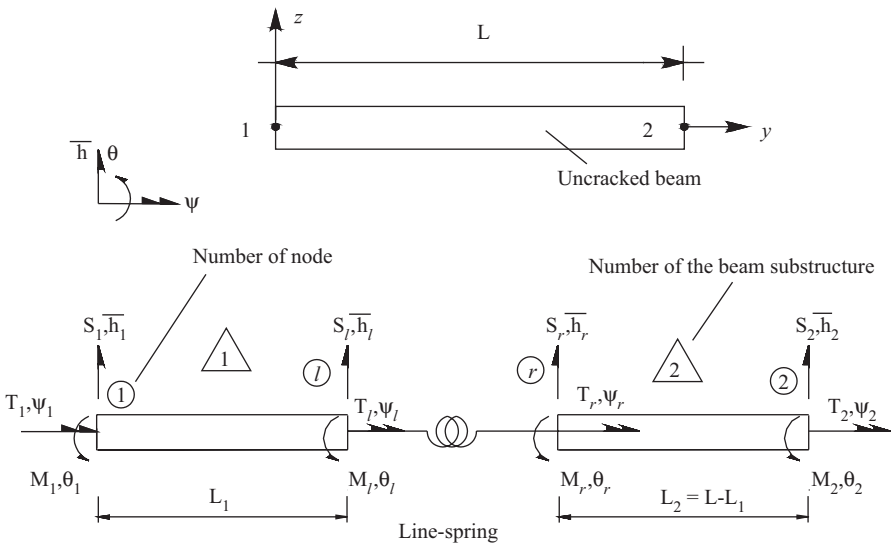

Fig. 4. Models of the uncracked beam, the two substructures with the line spring and the conditions for forces and displacements of the beam element.

crack from total stiffness, we have to introduce two additional nodes, namely nodes l and r, representing, respectively, the left- and right-hand sides of the crack faces. Because the length of the line spring is always zero, the two nodes l and r have the same y coordinate.

The line-spring model as applied to surface cracks initially assumes that the crack is a through-crack of the same length; shearing forces and bending and torsional moments are directly applied at the cracked section. Such forces and moments can be related to the deformation of the net ligament through compliance expressions, as if one were actually replacing the net ligament by "springs" connecting both faces of the crack. The "springs" have the features of having two nodes and zero length. Since they include the three degrees of freedom commonly associated with nodes in beam-column elements, they are easily incorporated into standard beam-column codes. The compliance expressions of such springs at any point along the crack are obtained from the plane-strain solution of an edge-cracked strip of width equal to the thickness of the beam and crack length equal to the surface crack depth at the particular point. In the vibration analysis of an edge-cracked beam, the aforementioned line-spring model should be slightly modified

so that the closure forces are replaced by shear forces. However, in this paper, the crack will always be considered open.

In an effort to determine the unknown shear forces and bending and torsional moments acting on the line spring, static equilibrium and compatibility conditions are enforced. That is, because the length of the line spring is always zero, the two nodes have the same y coordinate. As shown in Fig. 4, static equilibrium requires that

$$\begin{aligned} S_l &= S_r = S, \\ M_l &= M_r = M, \\ T_l &= T_r = T. \end{aligned} \tag{17}$$

Since the shear force S and the torsion T do not interact with the bending moment M in the zero-length line-spring model [20,21] the respective cross-compliances are zero. There is interaction only between the shear force S and the torsion T. In this case, the relative cross-compliances $\lambda_{st} = \lambda_{ts}$ are different from zero.

Nevertheless in the general case, the compatibility conditions due to the local flexibility of the crack are written as

$$\begin{aligned} \Theta &= \lambda_{mm} M + \lambda_{ms} S + \lambda_{mt} T, \\ H &= \lambda_{sm} M + \lambda_{ss} S + \lambda_{st} T, \\ \Psi &= \lambda_{tm} M + \lambda_{ts} S + \lambda_{tt} T \end{aligned} \tag{18}$$

in which the rotations Θ and Ψ and the deflection H across the line spring are expressed in terms of the nodal displacements:

$$\begin{aligned} \Theta &= \Theta_l - \Theta_r, \\ \Psi &= \Psi_l - \Psi_r, \\ H &= H_l - H_r, \end{aligned} \tag{19}$$

where λ_{mm}, λ_{ss}, λ_{tt} and $\lambda_{st} = \lambda_{ts}$, $\lambda_{ms} = \lambda_{sm}$, $\lambda_{tm} = \lambda_{mt}$ are the compliance coefficients, respectively, for bending moment, shear force and torsion.

Under general loading, the additional displacement u_i along the direction of force P_i due to the presence of the crack will be computed using Castigliano's theorem and by generalisation of the Paris equation.

To this end, if U is the strain energy due to the crack, Castigliano's theorem demands that the additional displacement be

$$u_i = \partial U / \partial P_i \tag{20}$$

along the force P_i. The strain energy [22–26] will have the form

$$U = \int_0^a \frac{\partial U}{\partial a}\,\mathrm{d}a = \int_0^a J\,\mathrm{d}a, \tag{21}$$

where a is the crack length and $J = \partial U/\partial a$ is the strain energy density function. Therefore,

$$u_i = \frac{\partial}{\partial P_i}\left[\int_0^a J(a)\,\mathrm{d}a\right] \quad \text{(Paris equation)}. \tag{22}$$

The flexibility coefficient λ_{ij} will be

$$\lambda_{ij} = \frac{\partial u_i}{\partial P_j} = \frac{\partial}{\partial P_i \partial P_j}\int_0^a J(a)\,\mathrm{d}a. \tag{23}$$

The strain energy density function J has the general form [26]

$$J = \frac{1}{E'}\left[\left(\sum_{q=1}^{3} K_{\mathrm{I}q}\right)^2 + \left(\sum_{q=1}^{3} K_{\mathrm{II}q}\right)^2 + \alpha\left(\sum_{q=1}^{3} K_{\mathrm{III}q}\right)^2\right], \tag{24}$$

where $E' = E$ for plane stress, $E' = E/(1-\nu^2)$ for plane strain, $\alpha = (1+\nu)$; E and ν are Young's modulus and Poisson's ratio, respectively. Then, integrating along the cut (z-axis):

$$\lambda_{ij} = \frac{1}{E'}\int_0^a \left[\frac{\partial^2}{\partial P_i \partial P_j}\sum_m \int_{-d/2}^{d/2} e_m \left(\sum_n K_{mn}\right)^2 \mathrm{d}z\right] \mathrm{d}a, \tag{25}$$

where d is the width of the T-section and $e_m = \alpha$ for $m = \mathrm{III}$ and $e_m = 1$ for $m = \mathrm{I}, \mathrm{II}$. Furthermore, K_{mn} is the stress intensity factor (SIF) of mode m ($m = \mathrm{I}, \mathrm{II}, \mathrm{III}$) due to the load P_n ($n = 1, 2, 3$) since the strain energy is additive.

Developing the sums

$$\lambda_{ij} = \frac{1}{E'}\int_0^a \frac{\partial^2}{\partial P_i \partial P_j}\left[\int_{-d/2}^{d/2}\left(\left(\sum_n K_{\mathrm{I}n}\right)^2 + \left(\sum_n K_{\mathrm{II}n}\right)^2 + \alpha\left(\sum_n K_{\mathrm{III}n}\right)^2\right)\mathrm{d}z\right]\mathrm{d}a \tag{26}$$

or

$$\lambda_{ij} = \frac{1}{E'}\int_0^a \frac{\partial^2}{\partial P_i \partial P_j}\left[\int_{-d/2}^{d/2}\left((K_{\mathrm{IS}} + K_{\mathrm{IM}} + K_{\mathrm{IT}})^2 + (K_{\mathrm{IIS}} + K_{\mathrm{IIM}} + K_{\mathrm{IIT}})^2 + \alpha(K_{\mathrm{IIIS}} + K_{\mathrm{IIIM}} + K_{\mathrm{IIIT}})^2\right)\mathrm{d}z\right]\mathrm{d}a.$$

For the T-beam under consideration, being $K_{\mathrm{I}S} = K_{\mathrm{I}T} = 0$, $K_{\mathrm{II}M} = K_{\mathrm{II}T} = 0$ and $K_{\mathrm{III}M} = 0$, the components of interest in the local flexibility matrix can be determined as

$$\lambda_{ss} = \frac{1}{E'}\int_0^a \left[\frac{\partial^2}{\partial S^2}\int_{-d/2}^{d/2}(K_{\mathrm{II}S}^2 + \alpha(K_{\mathrm{III}S})^2)\,\mathrm{d}z\right]\mathrm{d}a, \tag{27}$$

$$\lambda_{mm} = \frac{1}{E'}\int_0^a \frac{\partial^2}{\partial M^2}\int_{-d/2}^{d/2}(K_{IM})^2\,\mathrm{d}z\,\mathrm{d}a, \tag{28}$$

$$\lambda_{tt} = \frac{1}{E'}\int_0^a \frac{\partial^2}{\partial T^2}\int_{-d/2}^{d/2}\alpha K_{\mathrm{III}T}^2\,\mathrm{d}z\mathrm{d}\,a, \tag{29}$$

$$\lambda_{st} = \lambda_{ts} = \frac{1}{E'}\int_0^a \frac{\partial^2}{\partial S \partial T}\int_{-d/2}^{d/2}\alpha(K_{\mathrm{III}S}K_{\mathrm{III}T})\,\mathrm{d}z\,\mathrm{d}a. \tag{30}$$

It should be noted that for the T cross-section, the estimate of the SIFs is based on the simple method proposed in Ref. [27] for which

$$K_{\mathrm{I}M} = M_x\sqrt{\frac{\beta_M}{I_x h}\left(\frac{I_x}{I_x^c} - 1\right)}, \tag{31}$$

$$K_{\mathrm{II}S} = S_z\sqrt{\frac{\chi_z \beta_S}{dA}\left(\frac{A}{A^c} - 1\right)}, \tag{32}$$

$$K_{\mathrm{III}T} = T\sqrt{\frac{\beta_T}{dJ}\left(\frac{J}{J^c} - 1\right)}, \tag{33}$$

where I, I^c denote the moments of inertia, J, J^c, the polar moments of inertia and A, A^c the area of uncracked and cracked beam portion, respectively. The coefficients β_M, β_S and β_T are discussed and calculated in Ref. [27]. In fact, usually, adequate information is available for all K_{mn}, but, if the geometry of the cross-section is different from those represented in literature, the stress distribution in a beam is not known, as in the case of the T-cross-section subjected to a torsion T, or if the SIF is variable along the z-axis, as in the case of $K_{\mathrm{I}M}$, it is possible to evaluate the SIFs at the crack tips using the energy consideration of the cracked components.

The weight function method in the crack problem falls into this category. Clearly, the computing compliance method is an approach for evaluating SIFs, which is also based on the energy consideration [27].

From the discussion in Ref. [27], the torsion, the shear and the bending compliances imply an overall behaviour of the bar and not a local singular behaviour at the crack tip. In this case, the demand for solving the boundary value problem is not overcritical. It is proved that even though the singular behaviour of stress at the vicinity of the crack tip has not been modelled in computation, accurate results for SIFs can be obtained [28].

From the above-mentioned derivation we see that there are limitations to the suggested solution technique but the formulae appear to be handy for practicing engineers and designers to use in design and manufacturing processes.

Unfortunately, the same energetic considerations can not be immediately extended to the SIF $K_{\mathrm{III}S}$ which should be considered in Eqs. (27) and (30). It is not so easy to calculate a mode III SIF caused by the presence of the shear force S. We are working to find an appropriate expression for $K_{\mathrm{III}S}$ but, so far, we have not obtained satisfactory results.

Therefore, in this paper, we decided to consider the expression of the compliance λ_{ss} as a function of the SIF $K_{\mathrm{II}S}$ and to put λ_{st} equals to zero.

By means of Castigliano's theorem, the stiffness matrix of the line spring may be derived in Appendix A.

The stiffness matrix of a line spring $\mathbf{k}_f$ is given as follows:

$$\mathbf{k}_f = \begin{bmatrix} 1/\lambda_{ss} & 0 & 0 & -1/\lambda_{ss} & 0 & 0 \\ 0 & 1/\lambda_{mm} & 0 & 0 & -1/\lambda_{mm} & 0 \\ 0 & 0 & 1/\lambda_{tt} & 0 & 0 & -1/\lambda_{tt} \\ -1/\lambda_{ss} & 0 & 0 & 1/\lambda_{ss} & 0 & 0 \\ 0 & -1/\lambda_{mm} & 0 & 0 & 1/\lambda_{mm} & 0 \\ 0 & 0 & -1/\lambda_{tt} & 0 & 0 & 1/\lambda_{tt} \end{bmatrix}. \tag{34}$$

The formulation of a cracked beam element for structural analysis, as well as the crack effect on stability of beams under conservative and non-conservative forces have been investigated in Refs. [29–31].

The global DSM for the whole structure can now be assembled using the above dynamic stiffness matrices of all substructures and the line-spring stiffness matrix by applying the standard procedure of the finite element method.

The form of the DSM of the system of two substructures placed as shown in Fig. 4, and consisting of the line-spring element between the 1th and the 2th substructures of the beam-like structure is given as follows:

$$\mathbf{K}_g = \mathbf{K}^1 + \mathbf{K}_f + \mathbf{K}^2$$

$$= \begin{bmatrix} k^1_{11} & k^1_{12} & k^1_{13} & k^1_{14} & k^1_{15} & k^1_{16} & 0 & 0 & 0 & 0 & 0 & 0 \\ k^1_{21} & k^1_{22} & k^1_{23} & k^1_{24} & k^1_{25} & k^1_{26} & 0 & 0 & 0 & 0 & 0 & 0 \\ k^1_{31} & k^1_{32} & k^1_{33} & k^1_{34} & k^1_{35} & k^1_{36} & 0 & 0 & 0 & 0 & 0 & 0 \\ k^1_{41} & k^1_{42} & k^1_{43} & k^1_{44}+(1/\lambda_{ss}) & k^1_{45} & k^1_{46} & -1/\lambda_{ss} & 0 & 0 & 0 & 0 & 0 \\ k^1_{51} & k^1_{52} & k^1_{53} & k^1_{54} & k^1_{55}+(1/\lambda_{mm}) & k^1_{56} & 0 & -(1/\lambda_{mm}) & 0 & 0 & 0 & 0 \\ k^1_{61} & k^1_{62} & k^1_{63} & k^1_{64} & k^1_{65} & k^1_{66}+(1/\lambda_{tt}) & 0 & 0 & -1/\lambda_{tt} & 0 & 0 & 0 \\ 0 & 0 & 0 & -1/\lambda_{ss} & 0 & 0 & k^2_{11}+(1/\lambda_{ss}) & k^2_{12} & k^2_{13} & k^2_{14} & k^2_{15} & k^2_{16} \\ 0 & 0 & 0 & 0 & -(1/\lambda_{mm}) & 0 & k^2_{21} & k^2_{22}+(1/\lambda_{mm}) & k^2_{23} & k^2_{24} & k^2_{25} & k^2_{26} \\ 0 & 0 & 0 & 0 & 0 & -(1/\lambda_{tt}) & k^2_{31} & k^2_{32} & k^2_{33}+(1/\lambda_{tt}) & k^2_{34} & k^2_{35} & k^2_{36} \\ 0 & 0 & 0 & 0 & 0 & 0 & k^2_{41} & k^2_{42} & k^2_{43} & k^2_{44} & k^2_{45} & k^2_{46} \\ 0 & 0 & 0 & 0 & 0 & 0 & k^2_{51} & k^2_{52} & k^2_{53} & k^2_{54} & k^2_{55} & k^2_{56} \\ 0 & 0 & 0 & 0 & 0 & 0 & k^2_{61} & k^2_{62} & k^2_{63} & k^2_{64} & k^2_{65} & k^2_{66} \end{bmatrix}, \tag{35}$$

where $\mathbf{K}^1$ and $\mathbf{K}^2$ are the extended forms of dynamic stiffness matrices for the 1th and 2th uncracked substructures, respectively, and $\mathbf{K}_f$ is the stiffness matrix for the line-spring element expressed in the extended

form. It should be noted that, in order to enable the addition of elements of matrices (14) and (34) to the global system matrix, matrices must first be expanded so that they refer to all the degrees of freedom in the system.

The global DSM $\mathbf{K}_g$ obtained has a 12×12 dimension in this case (see Eq. (35)).

4. Modal parameter evaluations of cracked beams

Once the global DSM of the system is obtained, after introducing the boundary conditions at the ends of the beam, one finally obtains the frequency equation. The restrained global stiffness matrix is denoted by $\mathbf{K}_g^*(\omega)$. The natural frequencies are those values of ω for which

$$\mathbf{K}_g^*(\omega)\mathbf{A}_g^* = \mathbf{0}, \tag{36}$$

where $\mathbf{A}_g^*$ is the restrained vector of constants, which allow definition of the modal shapes, namely the vector of the nodal displacement amplitudes.

The necessary and sufficient condition for non-zero elements in the column vector $\mathbf{A}_g^*$ of Eq. (36) is that $\Delta = |\mathbf{K}_g^*(\omega)|$ shall be zero, and non-trivial solutions are calculated by imposing the vanishing of Δ:

$$\Delta = |\mathbf{K}_g^*(\omega)| = 0. \tag{37}$$

The nonlinear Eq. (37) is the frequency equation, which can be numerically solved to give the values of ω that make the determinant singular. For any non-trivial values of ω the expression for Δ given by Eq. (37) has been used in locating the natural frequencies by successively tracking the change of its sign (see, for example, Refs. [32–34]).

The only way of computing the natural frequencies of an infinite system is to vary ω in small steps, calculating the determinant of $\mathbf{K}_g$ at each step, and to seek the values which make the determinant zero. There are, however, numerous disadvantages and dangers in such a procedure. In fact, it is quite conceivable that even innocent-looking structures may have very close natural frequencies. To be sure of not missing any of them it is obvious that the step-size used for ω would have to be very small indeed. Finally, the determinant may change sign not only by passing through zero but also via infinity. Expanding the determinant Δ algebraically is quite a formidable task, but became feasible with recent advances in symbolic computing. Thus most of the work reported here, was carried out using the software MATLAB in expanding the determinant Δ, and more importantly in simplifying the expression for Δ.

Therefore, the required natural frequencies are given by the zeros of a plot of Δ versus ω. If Δ is calculated as ω is increased from zero by small increments $\delta\omega$, a change of sign of Δ is a necessary and sufficient condition for a natural frequency to have been passed. Clearly, the increment $\delta\omega$ must be less than the minimum separation of natural frequencies, as otherwise a pair of natural frequencies could be undetected due to them both lying between two consecutive values of ω. Therefore, $\delta\omega$ must be chosen carefully to avoid this danger. Moreover, the roots of the nonlinear Eq. (37) were also obtained by using the Matlab function fzero(·).

Once the frequencies of the cracked beam are found, the starting point to obtain the cracked mode shapes of the beam (see Eqs. (5)–(7)) is the derivation of the assumed shape functions for bending displacements $H^n = H^n(y)$, torsional rotation $\Psi^n = \Psi^n(y)$ and anticlockwise rotations $\Theta^n = \Theta^n(y)$ for each substructure. In this case $n = 1, 2$ is the number of the beam substructures.

These functions are developed so that they exactly satisfy, for each substructure ($n = 1, 2$) of the beam, the homogeneous equations of equilibrium of an unstressed beam. Moreover, the above functions must also satisfy certain conditions at the cracked section and at the ends of the substructure.

Because the dynamic stiffness matrices of the basic elements such as beams are exact, the number of modes predicted by the model is not limited by the number of degrees of freedom used in the model itself.

In spite of the apparent complexity of the frequency and mode shape equations given above, results for the degenerate case of the bending–torsion coupled Timoshenko beam and Bernoulli–Euler beam with x_α non-zero, i.e. with non-coincident mass and shear centre, can be obtained by substituting in the data $p^2 = 0$ and $p^2 = r^2 = s^2 = 0$, respectively. Note that any one or more of the terms p^2, r^2, s^2 which uniquely describe the

effect of axial load, rotatory inertia and shear deformation, respectively, can be set to zero, either individually or in any combination, to obtain the degenerate cases.

Additionally, when $x_\alpha = 0$, $p^2 = r^2 = s^2 = 0$, the computed DSM of Eqs. (35) gives the same stiffnesses as those of a Bernoulli–Euler beam.

5. Numerical examples

5.1. Frequency equation

A simple cantilever T-beam is used to demonstrate and validate the method outlined above. The material properties and other data used in the analysis are listed in Table 1. The end conditions for displacements and forces (see Fig. 4) for the cantilever beam are as follows:

$$\text{displacements}: \text{ at the built-in end } 1 \rightarrow (\xi_1 = 0): H_1 = 0, \Theta_1 = 0, \Psi_1 = 0, \tag{38}$$

$$\text{forces}: \text{ at the free end } 2 \rightarrow (\xi_2 = 1): S_2 = 0, M_2 = 0, T_2 = 0. \tag{39}$$

Substituting Eqs. (38) into Eqs. (5)–(7) and (39) into Eqs. (8)–(10) the end conditions for displacements and forces are applied at the built-in end 1 of the first uncracked substructure $\mathbf{K}^1$ and at the free end 2 of the second uncracked substructure $\mathbf{K}^2$ which compose the matrix $\mathbf{K}_g^*(\omega)$ together with the matrix $\mathbf{K}_f$. Once the global stiffness matrix $\mathbf{K}_g^*(\omega)$ has been obtained by using Eq. (36), one can calculate the natural frequencies of the cracked beam, as described in the previous section.

5.2. Mode shapes

If the crack is located a distance L_1 and L_2 from the left and right ends of the beam, respectively (see Fig. 5), the derivation of the shape functions (see Eqs. (5)–(7)) for bending displacements $H^n = H^n(y)$, torsional rotation $\Psi^n = \Psi^n(y)$ and anticlockwise rotations $\Theta^n = \Theta^n(y)$ $(n = 1, 2)$, is the starting point to obtain the cracked mode shapes of the beam.

Table 1
Material properties and other data used in the free vibration analysis of an axially loaded bending–torsion coupled Timoshenko beam

Beam parameter	Numerical value
E (N/m^2)	2.1×10^{11}
v	0.33
G (N/m^2)	78.94736×10^9
ρ (kg/m^3)	7800
h (m)	0.05
b (m)	0.05
d (m)	0.01
I (m^4)	19.638×10^{-8}
K	0.5
EI (N m^2)	41241.669
GJ (N m^2)	2368.421
m (kg/m)	7.02
I_α (kg m)	3.237×10^{-3}
x_α (m)	0.0111
L (m)	1.00
P (N)	15000
p^2	0.5237
r^2	1.5153×10^{-4}
s^2	8.0616×10^{-4}

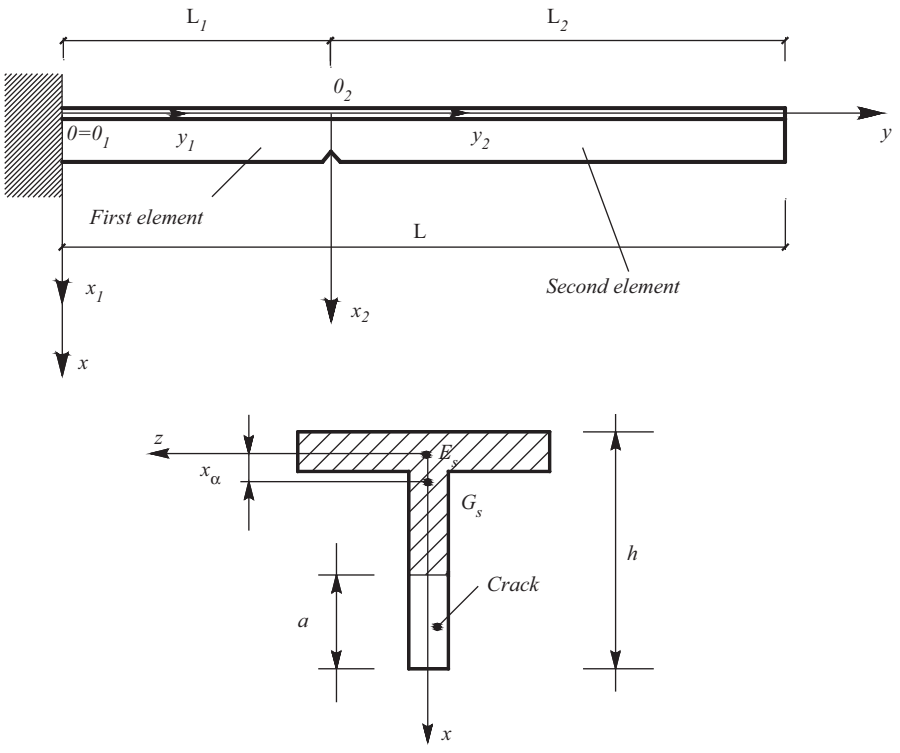

Fig. 5. Geometry and Cartesian coordinate systems of the cantilever beam with an edge crack and T-section.

In Fig. 5, a Cartesian coordinate system ($0xyz$) is defined. The y-axis is coincident with the centroidal axis of the uncracked beam, and x and z are coincident with the principal axes of the cross-section at the left end of the beam. The origin 0 of the coordinate system is at the intersection point between the centroidal axis and the left end cross-section.

Moreover, it may be useful to consider two other auxiliary coordinate systems, i.e., $0_1x_1y_1z_1$ and $0_2x_2y_2z_2$, as shown in Fig. 5, where z, z_1 and z_2 axes have to be considered orthogonally to the x–y plane.

The shape functions are developed so that they exactly satisfy, for each segment ($n = 1, 2$) of the beam, the homogeneous equations of equilibrium of an unstressed beam. Moreover, the above functions must also satisfy certain conditions at the cracked section and at the ends of the beam elements.

Displacements H and rotations Ψ and Θ may be described by

$$H^n(y) = \begin{cases} H^1(y_1) & 0 \leqslant y_1 \leqslant L_1, \\ H^2(y_2) & 0 \leqslant y_2 \leqslant L_2, \end{cases} \tag{40}$$

$$\Psi^n(y) = \begin{cases} \Psi^1(y_1) & 0 \leqslant y_1 \leqslant L_1, \\ \Psi^2(y_2) & 0 \leqslant y_2 \leqslant L_2, \end{cases} \tag{41}$$

$$\Theta^n(y) = \begin{cases} \Theta^1(y_1) & 0 \leqslant y_1 \leqslant L_1, \\ \Theta^2(y_2) & 0 \leqslant y_2 \leqslant L_2. \end{cases} \tag{42}$$

The three boundary conditions at the left end of the cantilever beam can be expressed as

$$\begin{aligned} H^1(y_1 = 0) &= 0, \\ \Psi^1(y_1 = 0) &= 0, \\ \Theta^1(y_1 = 0) &= 0. \end{aligned} \tag{43}$$

The three boundary conditions at the right end of the cantilever beam can be expressed as

$$S_2(y_2 = L_2) = 0,$$
$$M_2(y_2 = L_2) = 0,$$
$$T_2(y_2 = L_2) = 0. \tag{44}$$

At the crack location, $y_1 = L_1$ or $y_2 = 0$, where the elastic hinge is located, the local flexibility concept can be expressed as

(1) continuity of the bending moment:

$$M_l(y_1 = L_1) - M_r(y_2 = 0) = 0, \tag{45}$$

(2) continuity of the shear force:

$$S_l(y_1 = L_1) - S_r(y_2 = 0) = 0, \tag{46}$$

(3) continuity of the torsional moment:

$$T_l(y_1 = L_1) - T_r(y_2 = 0) = 0, \tag{47}$$

(4) discontinuity of the transverse displacement:

$$H^2(y_2 = 0) = H^1(y_1 = L_1) + \lambda_{ss} S_r(y_2 = 0), \tag{48}$$

(5) discontinuity of the cross-sectional rotation:

$$\Theta^2(y_2 = 0) = \Theta^1(y_1 = L_1) + \lambda_{mm} M_r(y_2 = 0), \tag{49}$$

(6) discontinuity of the torsional angle:

$$\Psi^2(y_2 = 0) = \Psi^1(y_1 = L_1) + \lambda_{tt} T_r(y_2 = 0). \tag{50}$$

For the beam in coupled bending–torsion, the crack will result in 6 additional boundary conditions at the crack location. Note that there is no coupling between the transverse displacement, the cross-sectional rotation and the torsional angle due to the presence of crack.

Substituting Eqs. (43)–(50) as required in Eqs. (5)–(7) and (8)–(10), written for $0 \leqslant \xi_1 \leqslant 1$ and $0 \leqslant \xi_2 \leqslant 1$, where $\xi_1 = y_1/L_1$ and $\xi_2 = y_2/L_2$, leads to the system of 12 homogeneous linear equations in 12 unknowns A_i ($i = 1, 2, \ldots, 12$) reported in Appendix B.

The modal vector is $\mathbf{A}_i$, in which one element may be fixed arbitrarily, and the remaining eleven constants can be solved in terms of the arbitrarily chosen one.

Thus, if A_1 is the chosen constant and the remaining constants A_2–A_{12} are expressed in terms of A_1, by using the symbolic computing package MATLAB, the mode shapes of the bending–torsion coupled beam are given in explicit form by rewriting Eqs. (40) and (41).

Once the 12 constants A_i ($i = 1, 2, \ldots, 12$) are found, substituting in the expressions of the bending displacements (Eq. (40)) and the torsional rotation (Eq. (41)) gives the displacements $H^n(y)$ and the torsional rotation $\Psi^n(y)$ for each substructure.

The first four natural frequencies of the uncracked and cracked cantilever beam obtained from $\Delta = |\mathbf{K}_g^*(\omega)| = 0$, with and without the inclusion of the effects of shear deformation and rotatory inertia, are given in Tables 2 and 3, respectively, for three different loading cases, namely when the axial load is zero ($P = 0$), tensile ($P = -15{,}000$ N) and compressive ($P = 15{,}000$ N), respectively. Note that the axial load applied is less than the 40% of the lowest uncoupled Euler critical buckling load of the cantilever. The cracked section is located at $L_1 = 0.5L$ distance from the built-in end and the crack depth is $a/h = 0.5$. Tables 2 and 3

Table 2
Natural frequencies of an uncracked axially bending–torsion coupled Timoshenko T-beam with cantilever end conditions

Frequency number (rad/s)	$P=0$ ($p^2=0$)		$P=15{,}000$ N ($p^2=0.5237$)		$P=-15{,}000$ N ($p^2=-0.5237$)	
	$r^2=s^2=0$	$r^2\neq0$, $s^2\neq0$	$r^2=s^2=0$	$r^2\neq0$, $s^2\neq0$	$r^2=s^2=0$	$r^2\neq0$, $s^2\neq0$
1	267.85	266.94	248.69	247.78	285.33	284.44
2	1478.23	1467.41	1467.9	1455.96	1487.83	1478.05
3	1762.46	1738.79	1750.41	1727.69	1775	1750.39
4	4080	3971.84	4064.5	3955.41	4095.36	3988.16

Table 3
Natural frequencies of a cracked axially bending–torsion coupled Timoshenko T-beam with cantilever end conditions, $L_1=0.5L$, $a/h=0.5$

Frequency number (rad/s)	$P=0$ ($p^2=0$)		$P=15{,}000$ N ($p^2=0.5237$)		$P=-15{,}000$ N ($p^2=-0.5237$)	
	$r^2=s^2=0$	$r^2\neq0$, $s^2\neq0$	$r^2=s^2=0$	$r^2\neq0$, $s^2\neq0$	$r^2=s^2=0$	$r^2\neq0$, $s^2\neq0$
1	179.103	178.755	118.75	118.49	219.67	219.22
2	842.227	837.1	814.88	808.8	866.22	862.13
3	1006.3	1000.14	994.82	989.65	1020.64	1013.01
4	3035.99	3012.5	3029.08	3005.11	3042.93	3019.86

show also the influence of rotatory inertia and/or shear deformation on the first four frequencies when $p^2=0$, $p^2<0$ and $p^2>0$. The frequencies given in Table 2 agree completely with published results [16,18,32] for the uncracked beam, i.e., compressive axial forces usually lower the natural frequencies, while tensile axial forces increase them. The results showing the effects of shear deformation, rotatory inertia and axial force are given in columns 5 and 7. As can be seen, the shear deformation did not make much difference for this particular problem investigated. The same considerations can be made for the cracked cantilever beam, as shown in Table 3. As expected, the frequencies related to the cracked beam are always lower than those of the uncracked beam. Some additional related studies can also be found in Refs. [35–37].

The plot of Δ against frequency (ω) which identifies the first three natural frequencies of the cracked beam is illustrated in Figs. 6(a)–(c), respectively, for three representative cases when (a) $P=0$, (b) $P=15{,}000$ N, and (c) $P=-15{,}000$ N, with $r^2\neq0$ and $s^2\neq0$.

Figs. 7–9 show the first four coupled bending–torsional modal shapes of the uncracked and cracked cantilever T-beams. In fact, plotting the bending displacements $H^1(\xi_1)$, $H^2(\xi_2)$ and the torsional displacements $x_\alpha\Psi^1(\xi_1)$, $x_\alpha\Psi^2(\xi_2)$, for the cracked cantilever beam, a comparison between the flexural displacements H and torsional displacements $x_\alpha\Psi$ of the uncracked beam, for $P=0$ with $r\neq0$, $s\neq0$, is given in these figures. In Figs. 7–9, in order to be consistent with the unit used for the bending displacement H and also to make the results more meaningful, the torsional rotation Ψ was multiplied by x_α. It should be noted that, $x_\alpha\Psi(\xi)$ represents the vertical displacements of the mass centre relative to the shear centre as a result of the twisting action.

Figs. 7–9 show that there is substantial coupling between bending displacements and torsional rotations in all the four modes.

To justified the discontinuity of the transverse displacement H and the product $x_\alpha\Psi$ at the cracked section, shown in Figs. 7–9, expressions (48) and (50) have to be considered.

Eqs. (48) and (50) show that the plot of the H and $x_\alpha\Psi$ functions is continuous only if the value of the products $\lambda_{ss}S_r(y_2=0)$ and $\lambda_{tt}T_r(y_2=0)$, at the cracked section, is zero. This means that the shear force $S_r(y_2=0)$ and the torsion $T_r(y_2=0)$ have to be zero, the coefficients λ_{ss} and λ_{tt} always being different from zero, at the cracked section. Figs. 10–12 plot the expression of the transverse displacement H and the product $x_\alpha\Psi$ for the first four modal shapes together with the behaviour of the shear force $S(\xi)$ and the torsion $T(\xi)$, when $r\neq0$, $s\neq0$ and $P=0$. For the modal shapes and the boundary conditions considered, the $S(\xi)$ and $T(\xi)$ expressions are always different from zero at the cracked section, even if, in the case of the first modal shape,

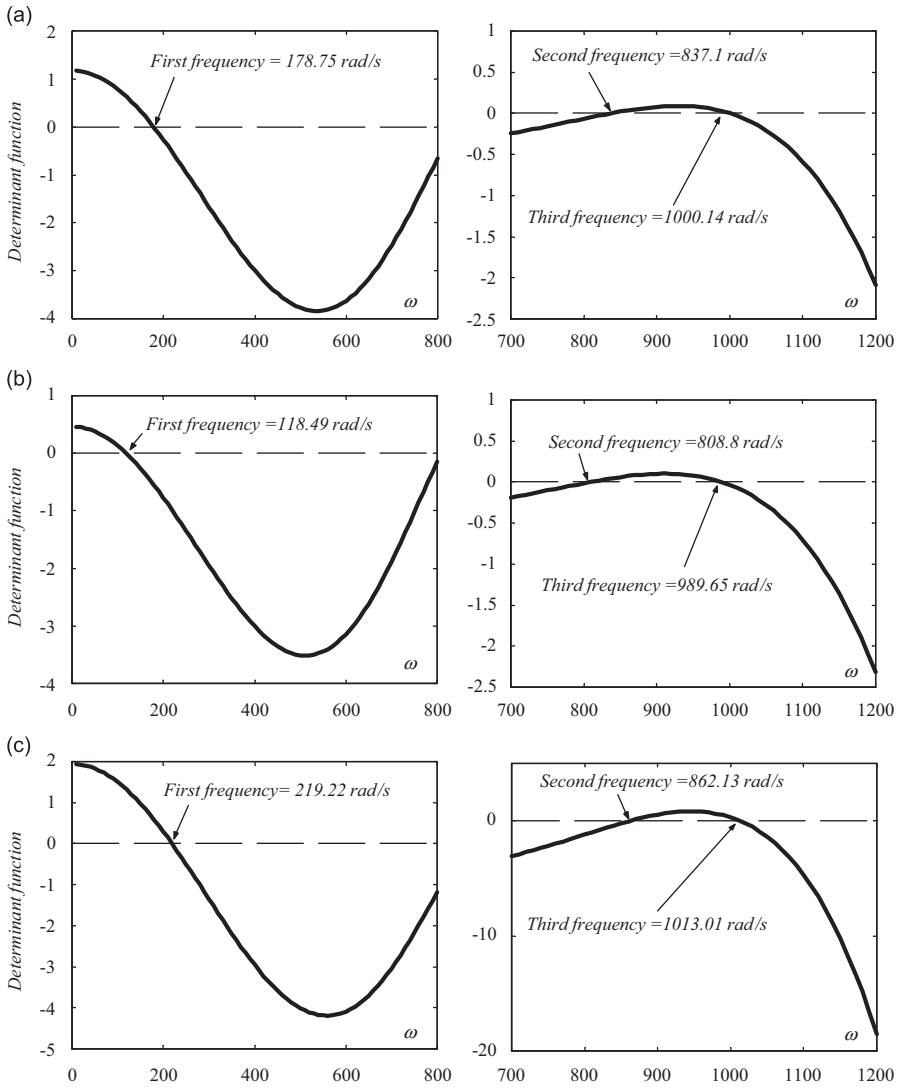

Fig. 6. Variation of the cracked cantilever beam determinant function with the frequency ω (rad/s) for the case when (a) $p^2 = 0$; $r \neq 0$, $s \neq 0$; (b) $p^2 > 0$; $r \neq 0$, $s \neq 0$; (c) $p^2 < 0$; $r \neq 0$, $s \neq 0$, $\xi = 0.5$, $a/h = 0.5$.

their values are so small that they had to be multiplied by 100 units. Therefore, the expressions of H and of the product Ψx_α are discontinuous at this section, depending on the values of the shear force, the torsion and the coefficients λ_{ss} and λ_{tt}. This is particularly evident in the fourth modal shape (see Fig. 12). In fact, at the cracked section, the value of the shear force $S_r(y_2 = 0)$ is bigger than the torsion $T_r(y_2 = 0)$. Being $\lambda_{tt} \gg \lambda_{ss}$, the discontinuity of the $x_\alpha \Psi$ function ($\lambda_{tt} T_r(y_2 = 0)$) is larger than that of the H function ($\lambda_{ss} S_r(y_2 = 0)$).

In Figs. 13–16, the variation of the first fourth bending modal shapes of the cracked cantilever beam are represented in succession as a function of the crack position together with those of the uncracked beam. In case A, the crack is located at $L_1 = 0.3L$ distance from the built-in end, in case B, $L_1 = 0.5L$ and in case C, $L_1 = 0.7L$. The crack depth is $a/h = 0.3$ in all these cases. The results displayed in these graphs reveal that the first frequencies are the lowest ones and are sensitive to the variation of the crack position. In this sense, when the crack is located closer to the beam root, the fundamental frequency is much lower than in the case of the crack located toward the beam tip. As concerns the implication of the position on the higher frequencies, these appear more complex than in the case of the fundamental frequency. The largest decreases of natural frequencies are experienced when the crack is located at positions of maximum curvature of the respective

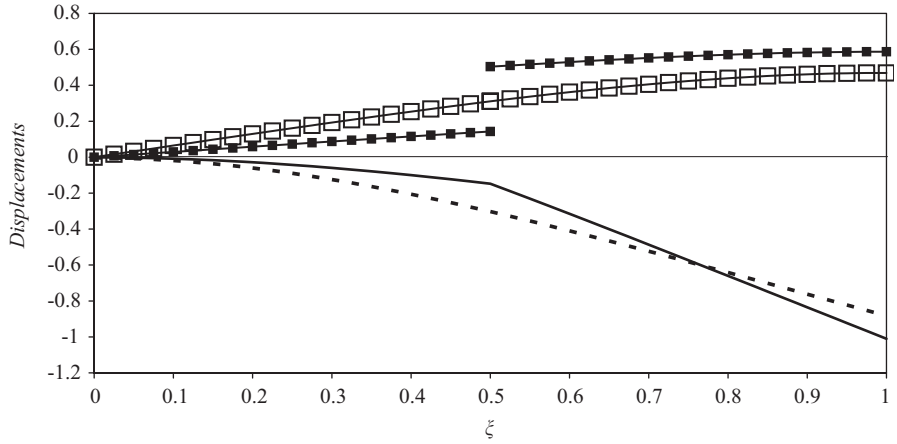

Fig. 7. First coupled bending–torsional modal shape of the uncracked and cracked cantilever T-beam: flexural displacements (H) and torsional displacements (Ψx_α) for $P = 0$, $r \neq 0$, $s \neq 0$. —— H; cracked beam; – – – H; uncracked beam; —■— $100\Psi x_\alpha$; cracked beam; —□— $100\Psi x_\alpha$; uncracked beam.

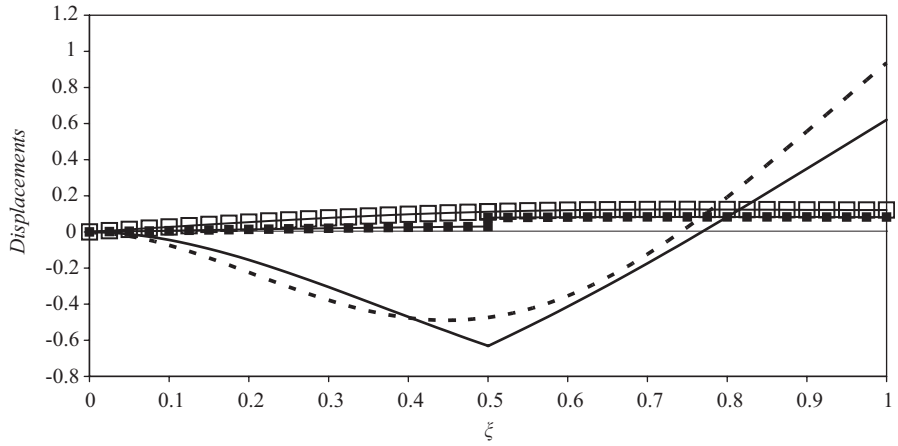

Fig. 8. Second coupled bending–torsional modal shape of the uncracked and cracked cantilever T-beam: flexural displacements (H) and torsional displacements (Ψx_α) for $P = 0$, $r \neq 0$, $s \neq 0$. —— H; cracked beam; – – – H; uncracked beam; —■— Ψx_α; cracked beam; —□— Ψx_α; uncracked beam.

modal shapes. When the crack is located at points of minimum curvature of modal shapes, the influence of the crack upon the natural frequencies is much smaller. For the second, third and fourth frequencies their variations depend strongly on how close the crack is to the nodal or antinodal points of the respective modal shapes. Indeed, in these figures the case of three cracks located according to the scenarios labelled as A–C, are considered. For the first natural frequency, it becomes clear that when the crack is remote from the root section, its value continuously increases. In this sense, it is readily seen that the fundamental frequency of case C is larger than in cases A and B, while the fundamental frequency corresponding to the case B is smaller than that corresponding to case C and larger than that of case A.

A change from this rule intervenes for the second, third and fourth frequencies, for cases A–C. In this sense, the results reveal, for example, that for case A, the second and third frequencies are not the lowest ones, but the ones associated with case B. Even in the case of the fourth modal frequency, the minimum one is that associated with case B. This change in trend can easily be explained by examining the variation of the corresponding modal shapes. From Figs. 13 to 16, for the second and third frequencies, it is readily

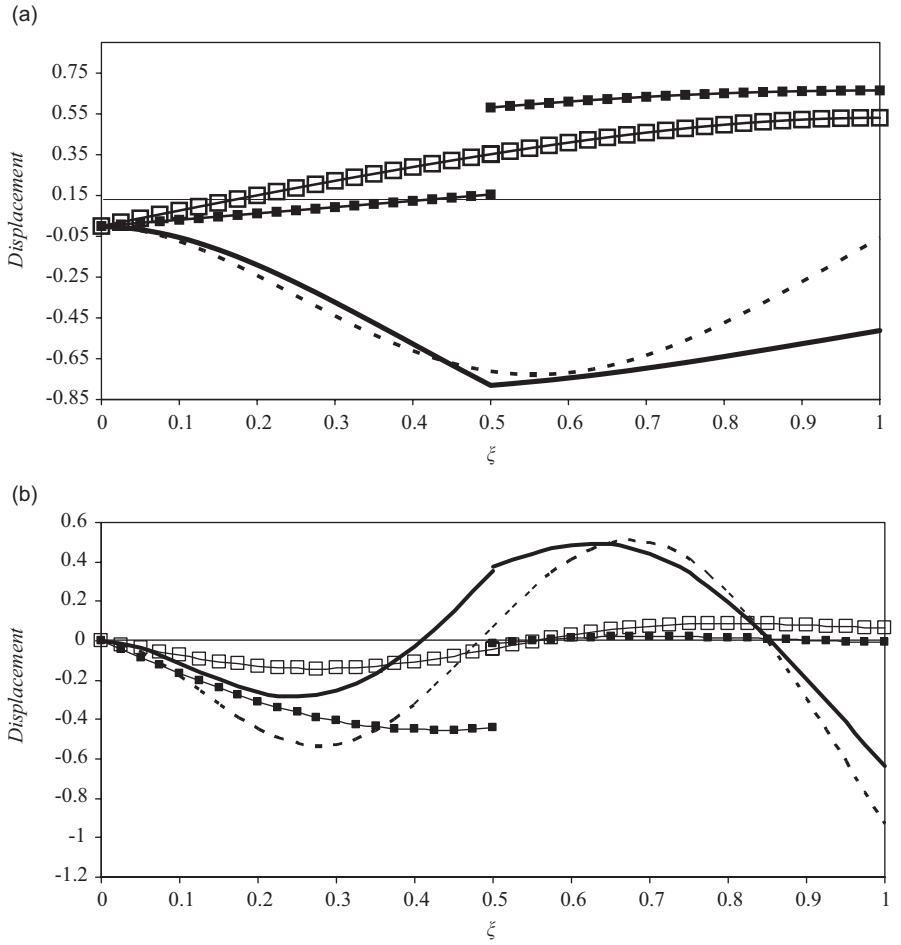

Fig. 9. Coupled bending–torsional modal shapes of the uncracked and cracked cantilever T-beam: (a) third modal shape (b) fourth modal shapes. Flexural displacements (H) and torsional displacements (Ψx_α) for $P = 0$, $r \neq 0$, $s \neq 0$. —— H; cracked beam; – – – H; uncracked beam; —■— Ψx_α; cracked beam; —□— Ψx_α; uncracked beam.

seen that for case B, in the region of the location of the crack, the maximum curvature of the corresponding modal shapes is experienced. The same conclusion can be obtained when examining the fourth modal shape associated with case B, that exhibits the minimum natural frequency even if, in this mode, when the crack is located at $L_1 = 0.3L$ (case A), the corresponding frequency is not very far from the one of the case B. In fact, for this position the crack is located at one point of local maximum curvature of the modal shape.

The first four bending modal shapes (H) corresponding to the various crack conditions are shown in Figs. 17–20, for the cracked and uncracked hinged–hinged beams having the same material properties and other data listed in Table 1. In this example, $P = 0$, $r^2 \neq 0$, $s^2 \neq 0$, the crack is located at $L_1 = 0.3L$ ($\xi = 0.3$) and $L_1 = 0.5L$ ($\xi = 0.5$) distances from the hinged end and two different crack depths have been considered, $a/h = 0.3$ and $a/h = 0.5$, respectively. As the deeper crack is closer to the antinodal point in the case of the first mode, the change in eigenfrequency with crack present is quite significant. But when the crack is located at $L_1 = 0.5\,L$, the second and third frequencies, for which the nodal points of the mode shapes are located at the midpoint of the span, give one more piece of information about the crack position: in fact, if the crack is located on a nodal point of a certain mode, the corresponding frequencies should be the same for all sizes of cracks and the same in turn as those for no crack. The nodal point of a flexural modal shape can be taken as point of inflection at which the bending moment vanishes. From Figs. 17 to 20, it can be

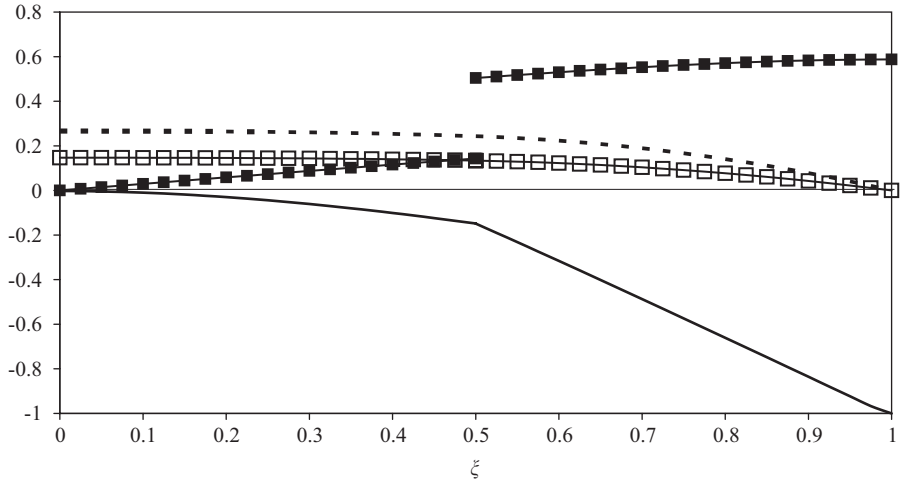

Fig. 10. Comparison between the vertical displacement H and the torsional rotation Ψx_α and the shear force $S(\xi)$ and the torsion $T(\xi)$ for the first modal shape of the cracked T-beam when $r\neq0$, $s\neq0$ and $P=0$, $\xi=0.5$, $a/h=0.5$. —— $H(\xi)$; −−− $100S(\xi)$; —■— $100\Psi x_\alpha(\xi)$; —□— $100T(\xi)$.

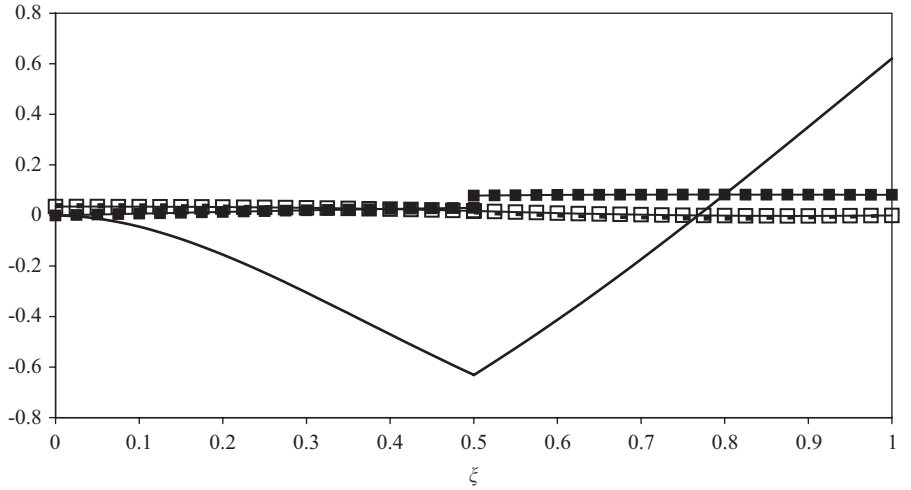

Fig. 11. Comparison between the vertical displacement H and the torsional rotation Ψx_α and the shear force $S(\xi)$ and the torsion $T(\xi)$ for the second modal shape of the cracked T-beam when $r\neq0$, $s\neq0$ and $P=0$, $\xi=0.5$, $a/h=0.5$. —— $H(\xi)$; −−− $S(\xi)$; —■— $\Psi x_\alpha(\xi)$; —□— $T(\xi)$.

seen that, in the case of bending–torsional coupled beam, this is not true. The frequencies corresponding to the cases of the uncracked beam and the cracked beam for which $L_1=0.5L$, $a/h=0.3$ and 0.5, are not the same. This effect is related to the presence of the torsion, which is different from zero at the section considered.

Plotting the bending displacements $H^1(\xi_1)$, $H^2(\xi_2)$ and the torsional displacements $x_\alpha\Psi^1(\xi_1)$, $x_\alpha\Psi^2(\xi_2)$, for the cracked cantilever beam, the first four modal shapes are shown in Figs. 21–23, for the case when $P=0$, $r^2\neq0$, $s^2\neq0$, $P=15{,}000\,\mathrm{N}$ $(P>0)$, $r^2\neq0$, $s^2\neq0$ and $P=-15{,}000\,\mathrm{N}$ $(P<0)$, $r^2\neq0$ and $s^2\neq0$.

From Tables 2 to 3 and Figs. 21 to 23, it is possible to see that the influence of the axial force P is bigger for the first frequency than for the higher frequencies. In fact, as can be seen, regarding flexural and torsional displacements, the influence of the axial forces on the first mode is visible, whereas the other modes are much less affected. Compressive axial forces are usually lower the natural frequencies, while tensile axial forces increase them. Therefore, a compressive axial force renders the beam less stiff, whereas a tensile one has a

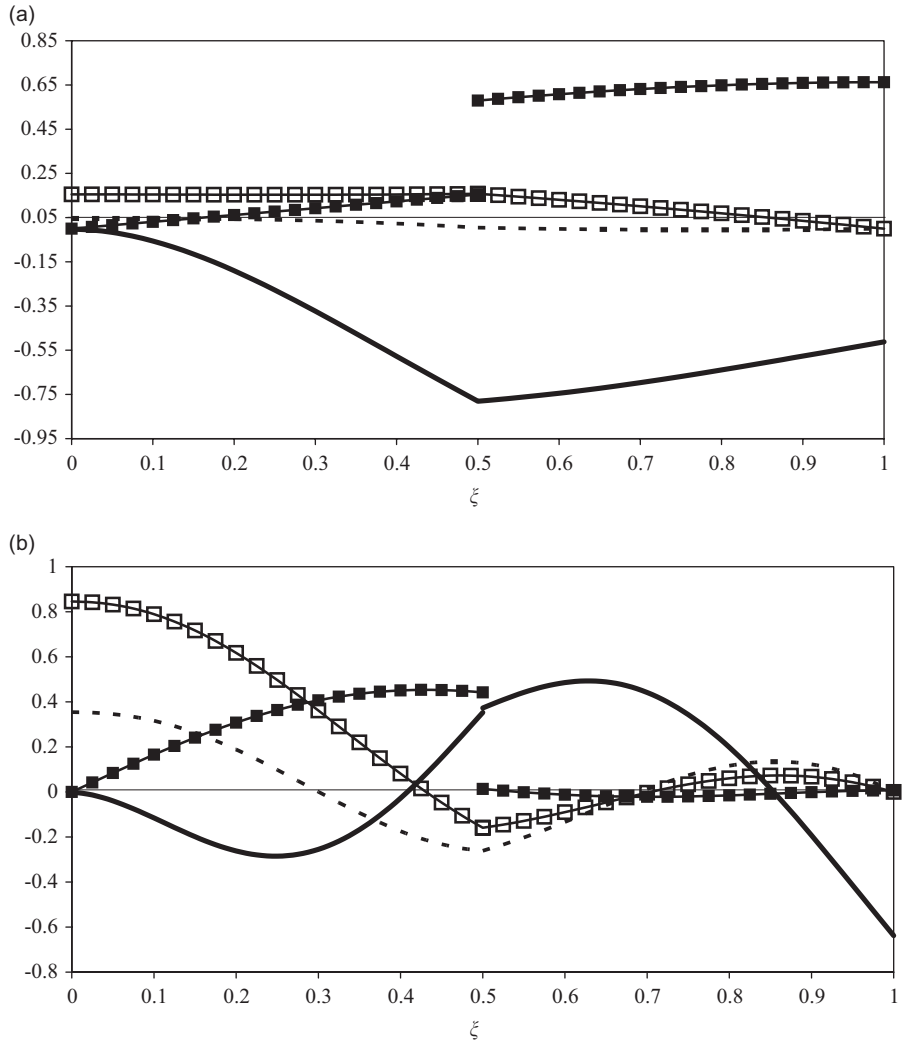

Fig. 12. Comparison between the vertical displacement H and the torsional rotation Ψx_α and the shear force $S(\xi)$ and the torsion $T(\xi)$ for (a) the third and (b) the fourth modal shapes of the cracked T-beam when $r\neq0$, $s\neq0$ and $P=0$, $\xi=0.5$, $a/h=0.5$. —— $H(\xi)$; −−− $S(\xi)$; —■— $\Psi x_\alpha(\xi)$; —□— $T(\xi)$.

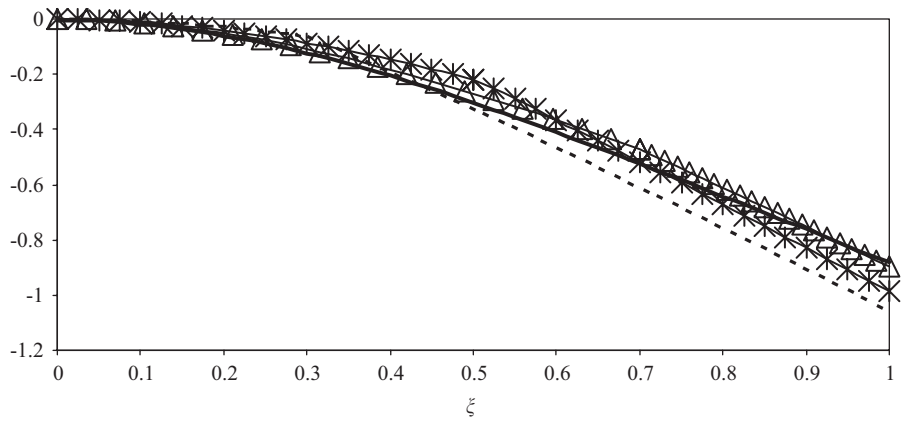

Fig. 13. Variation of the first bending modal shapes (H) for the case of the uncracked cantilever beam and of three cracks distributed differently, as indicated ($a/h=0.3$). −−− 179.66 rad/s (A: $L_1=0.3L$); —✳— 224.65 rad/s (B: $L_1=0.5L$); —△— 258.46 rad/s (C: $L_1=0.7L$); —— 266.94 rad/s (*uncracked beam*) for $P=0$; $r\neq0$, $s\neq0$.

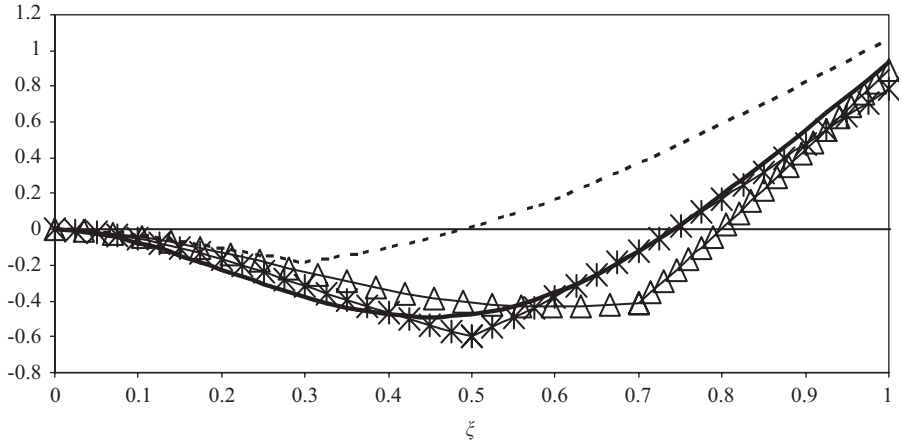

Fig. 14. Variation of the second bending modal shapes (H) for the case of the uncracked cantilever beam and of three cracks distributed differently, as indicated ($a/h = 0.3$). – – – 1090.55 rad/s (A: $L_1 = 0.3L$); —✳— 1055 rad/s (B: $L_1 = 0.5L$); —△— 1134.45 rad/s (C: $L_1 = 0.7L$); —— 1467.41 rad/s (*uncracked beam*) for $P = 0$; $r \neq 0$, $s \neq 0$.

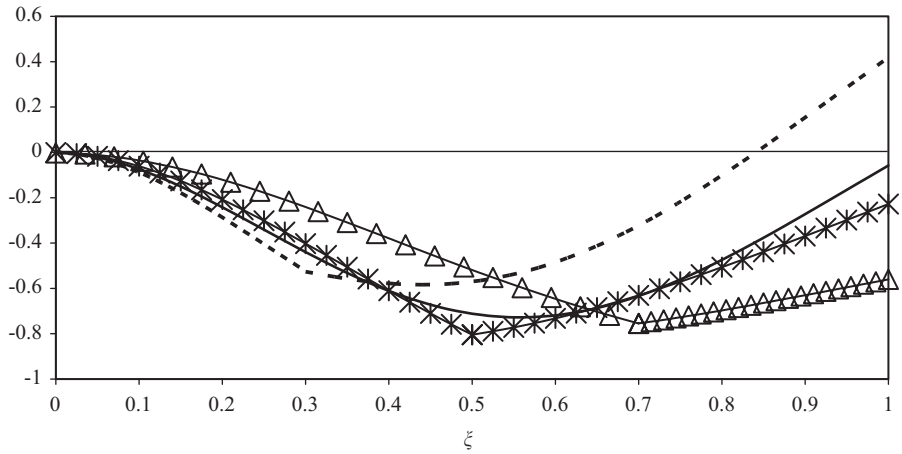

Fig. 15. Variation of the third bending modal shapes (H) for the case of the uncracked cantilever beam and of three cracks distributed differently, as indicated ($a/h = 0.3$). – – – 1576.93 rad/s (A: $L_1 = 0.3L$); —✳— 1297.71 rad/s (B: $L_1 = 0.5L$; —△— 1414.13 rad/s (C: $L_1 = 0.7L$); —— 1738.79 rad/s (*uncracked beam*) for $P = 0$; $r \neq 0$, $s \neq 0$.

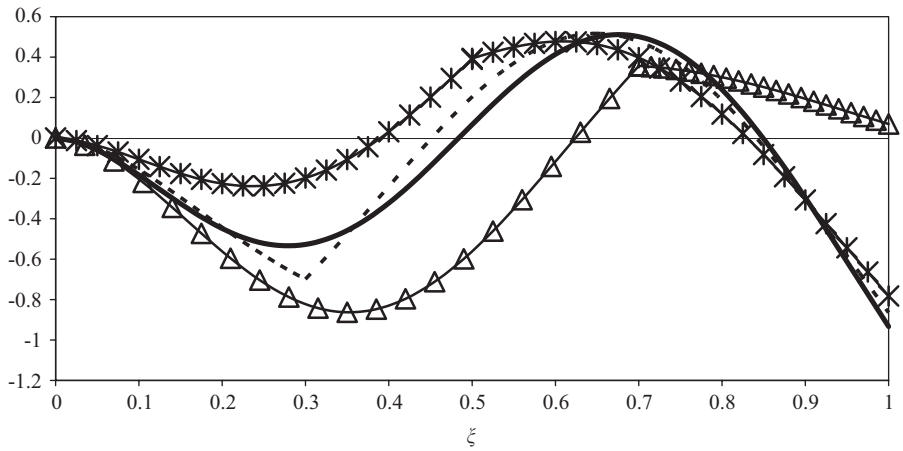

Fig. 16. Variation of the fourth bending modal shapes (H) for the case of the uncracked cantilever beam and of three cracks distributed differently, as indicated ($a/h = 0.3$). – – – 3411.21 rad/s (A: $L_1 = 0.3L$); —✳— 3340.20 rad/s (B: $L_1 = 0.5L$); —△— 3693.42 rad/s (C: $L_1 = 0.7L$); —— 3971.84 rad/s (*uncracked beam*) for $P = 0$; $r \neq 0$, $s \neq 0$.

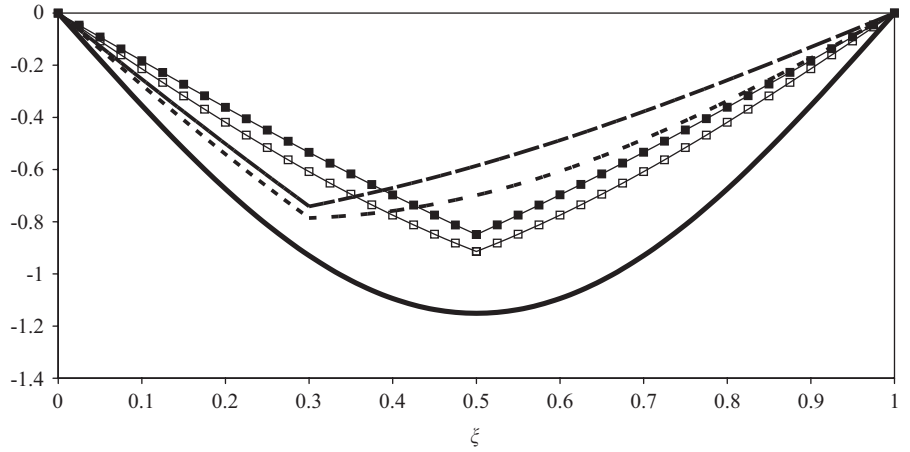

Fig. 17. First bending modal shapes (H) for the uncracked and cracked hinged–hinged beam as a function of the crack positions $\xi = 0.3$ and 0.5 and the depths $a/h = 0.3$ and $a/h = 0.5$. — — 847.9 rad/s (*uncracked beam*): – – – 571.78 rad/s ($a/h = 0.3$, $\xi = 0.3$); ——— 397.32 rad/s ($a/h = 0.5$, $\xi = 0.3$); —■— 342.4 rad/s ($a/h = 0.5$, $\xi = 0.5$); —□— 509.50 rad/s ($a/h = 0.3$, $\xi = 0.5$), for $P = 0$; $r \neq 0$, $s \neq 0$.

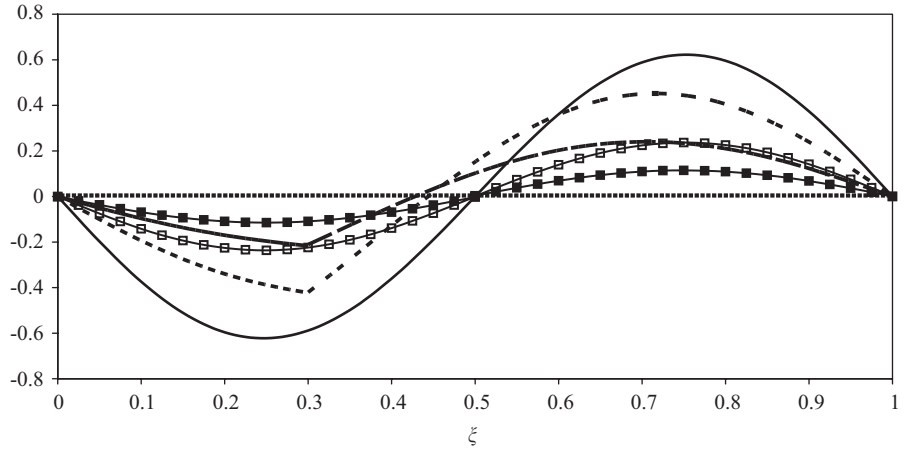

Fig. 18. Second bending modal shapes (H) for the uncracked and cracked hinged–hinged beam as a function of the crack positions $\xi = 0.3$ and 0.5 and the depths $a/h = 0.3$ and $a/h = 0.5$. — — 2333.59 rad/s (*uncracked beam*): – – – 1753.73 rad/s ($a/h = 0.3$, $\xi = 0.3$); ——— 1279.32 rad/s ($a/h = 0.5$, $\xi = 0.3$); —■— 1195.4 rad/s ($a/h = 0.5$, $\xi = 0.5$); —□— 1717.32 rad/s ($a/h = 0.3$, $\xi = 0.5$), for $P = 0$; $r \neq 0$, $s \neq 0$.

stiffening effect [38]. So, in the absence of axial forces, the first frequencies are higher than the frequencies calculated for a compressive load and lower than those for a tensile load.

A justification of the influence of the axial force on the first modal shape (see Fig. 7) is related to the fact that it is predominantly a bending mode. In the plot of the first modal shape, shown in Fig. 7, it is possible to see that the values of the torsional displacements $x_\alpha \Psi(\xi)$ had to be multiplied by 100 units to be visible and comparable, in the figure, with the flexural displacements H. It means that, in the first modal shape, the influence of the torsion is very low.

Fig. 23(b) shows that, for the cracked cantilever beam considered, the influence of the axial force P is almost negligible in the fourth modal shape.

6. Conclusions

The analysis of the natural vibrations and modal shapes of cracked axially loaded bending–torsional coupled Timoshenko T-beams has been presented. When the effects of shear deformation and rotatory inertia

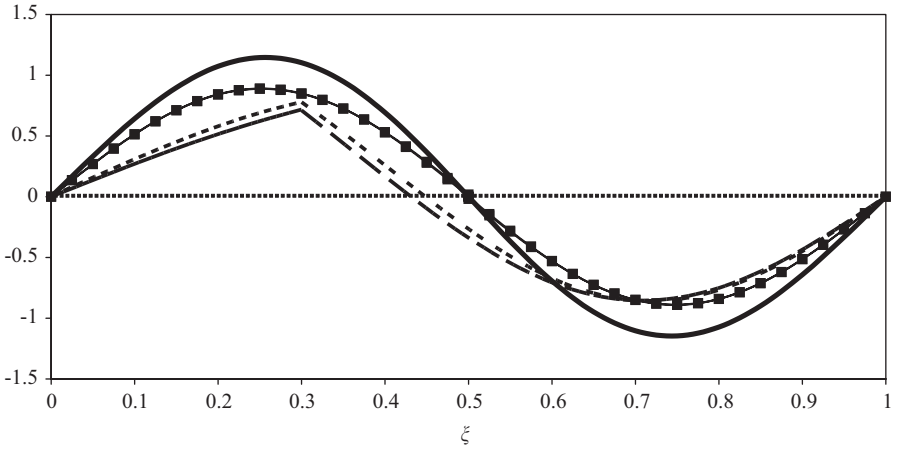

Fig. 19. Third bending modal shapes (H) for the uncracked and cracked hinged–hinged beam as a function of the crack positions $\xi = 0.3$ and 0.5 and the depths $a/h = 0.3$ and 0.5. — — 3725.83 rad/s (*uncracked beam*): – – – 2705.45 rad/s ($a/h = 0.3$, $\xi = 0.3$); ——— 2327.92 rad/s ($a/h = 0.5$, $\xi = 0.3$); —■— 3370.15 rad/s ($a/h = 0.5$, $\xi = 0.5$); —□— 3485.36 rad/s ($a/h = 0.3$, $\xi = 0.5$); for $P = 0$; $r \neq 0$, $s \neq 0$.

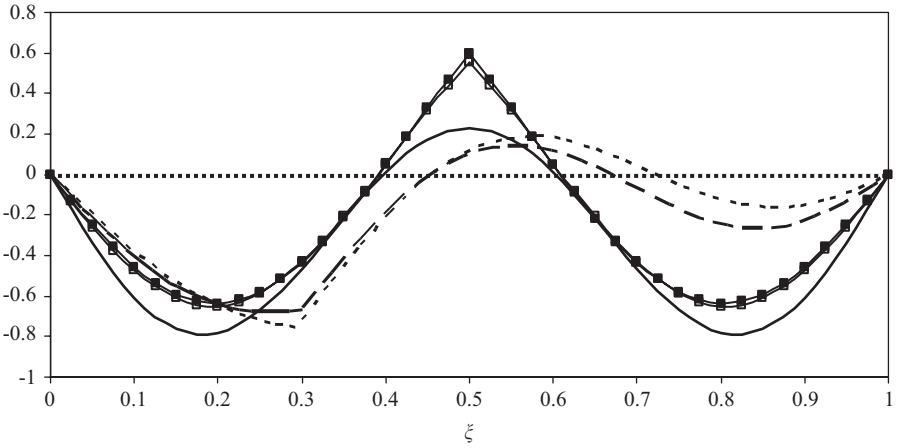

Fig. 20. Fourth bending modal shapes (H) for the uncracked and cracked hinged–hinged beam as a function of the crack positions $\xi = 0.3$ and 0.5 and the depths $a/h = 0.3$ and $a/h = 0.5$. — — 5011.03 rad/s (*uncracked beam*): – – – 4216.21 rad/s ($a/h = 0.3$, $\xi = 0.3$); ——— 4012.66 rad/s ($a/h = 0.5$, $\xi = 0.3$); —■— 4427.42 rad/s ($a/h = 0.5$, $\xi = 0.5$); —□— 4575.28 rad/s ($a/h = 0.3$, $\xi = 0.5$); for $P = 0$; $r \neq 0$, $s \neq 0$.

are neglected, the errors associated with them become increasingly large as the beams thickness increases and as the modal index increases. The general effect of including shearing effects is to decrease the natural frequencies. Some accurate data, which might be useful for others researchers to compare their results have been presented for uncracked and cracked T-beams. In the present study the transverse crack has always been considered as open, whether in the presence of an axial force or not.

The stiffness matrix is obtained within the context of the DSM method by directly solving the governing differential equation. In order to determine the local flexibility characteristics induced by an individual crack, the concept of the massless rotational spring is applied. A new procedure based on the coupling of DSM and line-spring element is introduced to model the cracked beam. The whole structure is first divided into two substructures, since only one crack is considered into the structure itself. For each substructure, the DSM is obtained, and the global DSM of the whole structure can be deduced by applying the standard procedure of the finite element method. The existence of a crack results in a reduction of the local stiffness, and this additional flexibility also alters the global dynamic response. In this sense, the results obtained have revealed

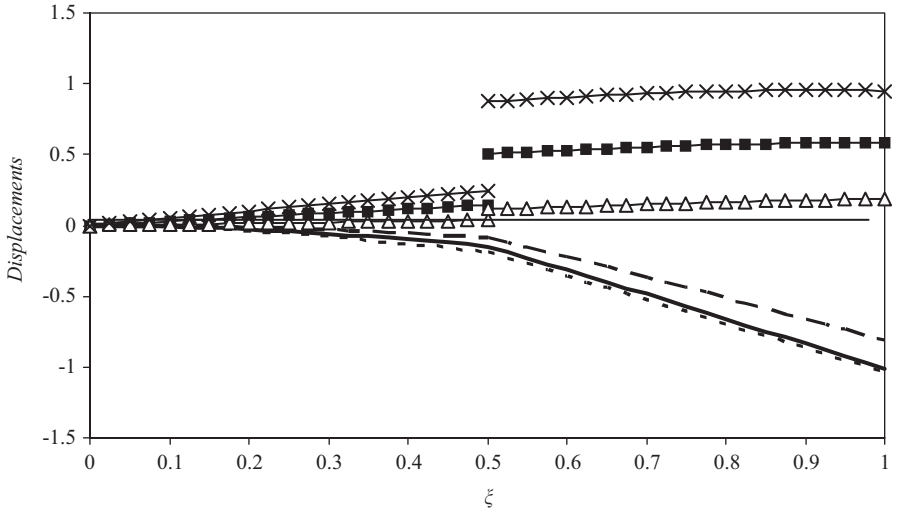

Fig. 21. First coupled bending–torsional modal shape of the cracked T-beam: flexural displacement (H) and torsional displacement (Ψx_α) for $r\neq0$, $s\neq0$, crack position $\xi = 0.5$, crack depth $a/h = 0.5$. —— H; $P = 0$: – – – H; $P<0$; — — H; $P>0$; —■— $100\Psi x_\alpha$; $P = 0$; —×— $100\Psi x_\alpha$; $P<0$; —△— $100\Psi x_\alpha$; $P>0$.

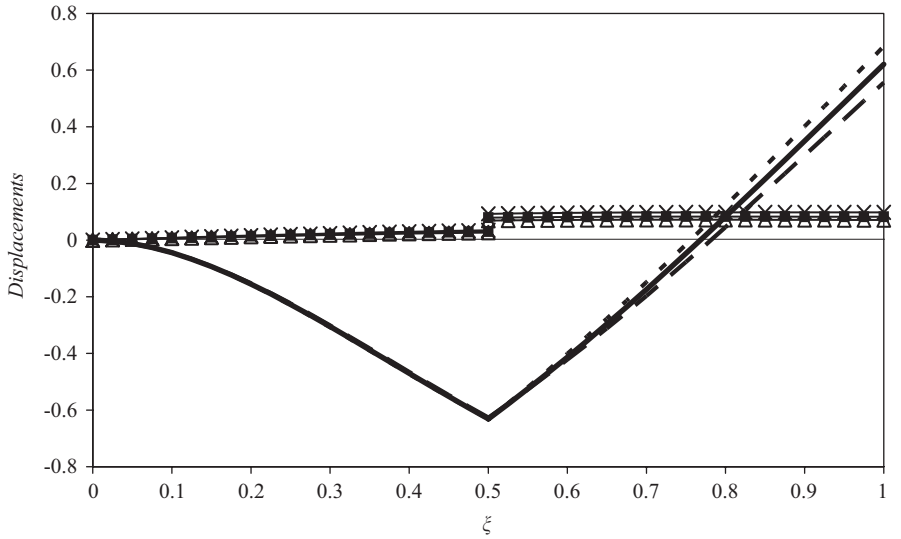

Fig. 22. Second coupled bending–torsional modal shape of the cracked T-beam: flexural displacement (H) and torsional displacement (Ψx_α) for $r\neq0$, $s\neq0$, crack position $\xi = 0.5$, crack depth $a/h = 0.5$. —— H; $P = 0$: – – – H; $P<0$; — — H; $P>0$; —■— Ψx_α; $P = 0$; —×— Ψx_α; $P<0$; —△— Ψx_α; $P>0$.

that a good prediction of changes in frequencies and mode shapes can contribute to the determination of the location and size of cracks.

A parametric study has been conducted considering two beams having different end conditions, a cantilever and a hinged–hinged beam, different crack positions and depths. The following observations can be made from the parametric study:

1. Any variation in the frequency of a mode is larger if the crack is closer to the nodal or the antinodal point of that mode shape. When the crack is located at the nodal point of a certain mode, the corresponding

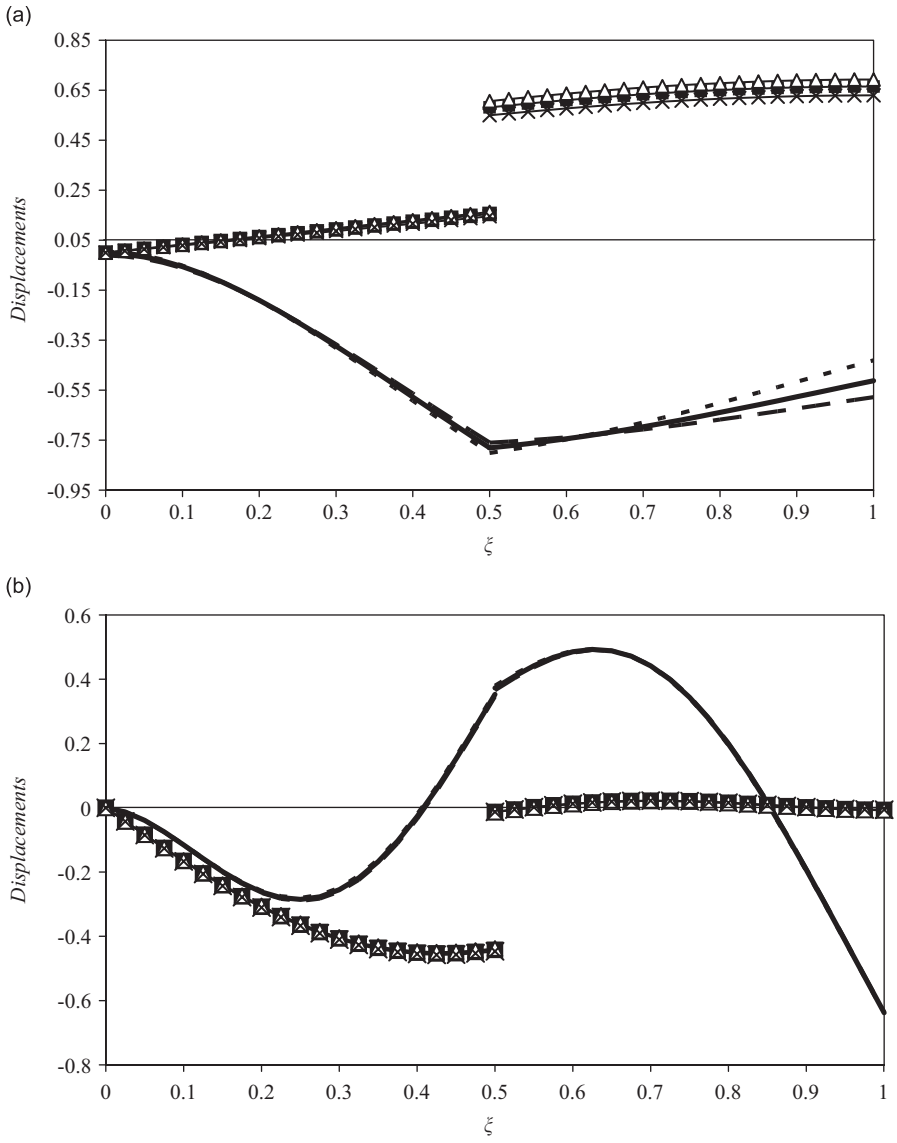

Fig. 23. (a) Third and (b) fourth coupled bending–torsional modal shapes of the cracked T-beam: flexural displacement (H) and torsional displacement (Ψx_α) for $r \neq 0$, $s \neq 0$, crack position $\xi = 0.5$, crack depth $a/h = 0.5$. —— H; $P = 0$: – – – H; $P < 0$; — — H; $P > 0$; —■— Ψx_α; $P = 0$; —×— Ψx_α; $P < 0$; —△— Ψx_α; $P > 0$.

frequencies are not the same for all sizes of cracks and the same in turn as those for no crack. So, even if the nodal point of a mode shape can be taken as point of inflection at which the bending moment vanishes, the value of the torsion determines different values of the frequency.

2. It can be noticed that when cracks of different depths are considered, the larger crack has the more significant effect on the frequency.
3. The frequency of the uncracked and cracked beam is also reduced because of compressive axial loads, while it increases with tensile loads, although not as fast as it reduces with compressive loads.

As far as the effect of the axial force is concerned, the aim of the authors is to demonstrate that, even in the case of cracked beams, the effect of a compressive axial force is to render the beam less stiff, whereas a tensile one has a stiffening effect.

In this work, warping stiffness has been neglected. The aim of the authors is to extend in a future paper the analysis of coupled vibrations of cracked Timoshenko beams including the effect of warping, as well as the coupling effects at the cracked section.

Acknowledgements

This research was supported by the MIUR (Italian Ministry for University and Scientific, Technological Research). The research theme is one of the topics of the Centre of Study and Research for the Identification of Materials and Structures (CIMEST)—"M. Capurso", of the University of Bologna.

Appendix A. Determination of the stiffness matrix of a line-spring model

Let us consider a model to evaluate the stiffness matrix $\mathbf{k}_f$ of a line spring, as shown in Fig. 4 which indicates the sign convections for forces (shear forces: S_l and S_r; bending moments M_l and M_r; torsion T_l and T_r). The corresponding deflections and rotations are respectively denoted by H_l and H_r; Θ_l and Θ_r; and Ψ_l and Ψ_r. Then the following relation is obtained:

$$\mathbf{F}_f = \mathbf{k}_f \mathbf{q}_f, \tag{A.1}$$

where

$$\mathbf{F}_f = [S_r, M_r, T_r, S_l, M_l, T_l]^{\mathrm{T}}, \quad \mathbf{q}_f = [H_r, \Theta_r, \Psi_r, H_l, \Theta_l, \Psi_l]^{\mathrm{T}}. \tag{A.2}$$

For a linear elastic body under an infinitesimal small displacement condition, the displacements u_i at the loading points can be written as follows using the principle of superposition:

$$u_i = \sum_{j=1}^{n} \lambda_{ij} P_j, \tag{A.3}$$

where P_j are generalised forces and λ_{ij} are compliances. From Eq. (A.3), the deflection H at the point where a shear force S is applied can be written by considering the effects of both a bending moment M and a torsion T as

$$H = \lambda_{ss} S + \lambda_{sm} M + \lambda_{st} T. \tag{A.4}$$

Similarly, it is possible to obtain

$$\Theta = \lambda_{ms} S + \lambda_{mm} M + \lambda_{mt} T, \tag{A.5}$$

$$\Psi = \lambda_{ts} S + \lambda_{tm} M + \lambda_{tt} T. \tag{A.6}$$

With the following positions for displacements, forces and compliances

$$\begin{aligned}
&u_1 = H; \quad P_1 = S, \\
&u_2 = \Theta; \quad P_2 = M, \\
&u_3 = \Psi; \quad P_3 = T, \\
&\lambda_{11} = \lambda_{ss} \quad \lambda_{21} = \lambda_{ms} \quad \lambda_{31} = \lambda_{ts}, \\
&\lambda_{12} = \lambda_{sm} \quad \lambda_{22} = \lambda_{mm} \quad \lambda_{32} = \lambda_{tm}, \\
&\lambda_{13} = \lambda_{st} \quad \lambda_{23} = \lambda_{mt} \quad \lambda_{33} = \lambda_{tt},
\end{aligned} \tag{A.7}$$

where $\lambda_{ij} = \lambda_{ji}$ for $i, j = 1, 2, 3$.

The strain energy W in the line spring is given by

$$W = \frac{1}{2}(SH + M\Theta + T\Psi) \text{ or } W = \frac{1}{2}\sum_{i=1}^{3} P_i u_i. \tag{A.8}$$

It is possible to obtain another expression of W by substituting Eqs. (A.4)–(A.6) into Eq. (A.8):

$$W = \frac{1}{2D}(a_{11}H^2 + a_{22}\Theta^2 + a_{33}\Psi^2 + 2a_{12}H\Theta + 2a_{13}H\Psi + 2a_{23}\Theta\Psi), \tag{A.9}$$

where

$$\begin{aligned} a_{11} &= \lambda_{mm}\lambda_{tt} - \lambda_{mt}^2 \quad & a_{12} &= \lambda_{mt}\lambda_{st} - \lambda_{sm}\lambda_{tt}, \\ a_{22} &= \lambda_{pp}\lambda_{tt} - \lambda_{pt}^2 \quad & a_{13} &= \lambda_{sm}\lambda_{mt} - \lambda_{st}\lambda_{mm}, \\ a_{33} &= \lambda_{mm}\lambda_{pp} - \lambda_{mp}^2 \quad & a_{23} &= \lambda_{sm}\lambda_{st} - \lambda_{mt}\lambda_{ss}, \end{aligned}$$

$$D = \det\begin{bmatrix} \lambda_{ss} & \lambda_{sm} & \lambda_{st} \\ \lambda_{ms} & \lambda_{mm} & \lambda_{mt} \\ \lambda_{ts} & \lambda_{tm} & \lambda_{tt} \end{bmatrix}. \tag{A.10}$$

Using the relations $H = H_l - H_r$, $\Theta = \Theta_l - \Theta_r$, $\Psi = \Psi_l - \Psi_r$, one can express the strain energy W with nodal displacements and obtain the following relations by partial differentiation with respect to each nodal displacement:

$$S_l = \frac{\partial W}{\partial H_l} = [a_{11}(H_l - H_r) + a_{12}(\Theta_l - \Theta_r) + a_{13}(\Psi_l - \Psi_r)], \tag{A.11}$$

$$M_l = \frac{\partial W}{\partial \Theta_l} = [a_{12}(H_l - H_r) + a_{22}(\Theta_l - \Theta_r) + a_{23}(\Psi_l - \Psi_r)], \tag{A.12}$$

$$T_l = \frac{\partial W}{\partial \Psi_l} = [a_{13}(H_l - H_r) + a_{23}(\Theta_l - \Theta_r) + a_{33}(\Psi_l - \Psi_r)], \tag{A.13}$$

$$S_r = \frac{\partial W}{\partial H_r} = -S_l, \tag{A.14}$$

$$M_r = \frac{\partial W}{\partial \Theta_r} = -M_l, \tag{A.15}$$

$$T_r = \frac{\partial W}{\partial \Psi_r} = -T_l. \tag{A.16}$$

Thus the stiffness matrix of a line spring is given as follows:

$$\mathbf{k}_f = \frac{1}{D}\begin{bmatrix} a_{11} & a_{12} & a_{13} & -a_{11} & -a_{12} & -a_{13} \\ & a_{22} & a_{23} & -a_{21} & -a_{22} & -a_{23} \\ & & a_{33} & -a_{31} & -a_{32} & -a_{33} \\ & & & a_{11} & a_{12} & a_{13} \\ & \text{Sym} & & & a_{22} & a_{23} \\ & & & & 0 & a_{33} \end{bmatrix}. \tag{A.17}$$

For the case under consideration, being $\lambda_{mt} = \lambda_{ms} = \lambda_{st} = 0$, the stiffness matrix becomes

$$\mathbf{k}_f = \begin{bmatrix} 1/\lambda_{ss} & 0 & 0 & -1/\lambda_{ss} & 0 & 0 \\ 0 & 1/\lambda_{mm} & 0 & 0 & -1/\lambda_{mm} & 0 \\ 0 & 0 & 1/\lambda_{tt} & 0 & 0 & -1/\lambda_{tt} \\ -1/\lambda_{ss} & 0 & 0 & 1/\lambda_{ss} & 0 & 0 \\ 0 & -1/\lambda_{mm} & 0 & 0 & 1/\lambda_{mm} & 0 \\ 0 & 0 & -1/\lambda_{tt} & 0 & 0 & 1/\lambda_{tt} \end{bmatrix}. \tag{A.18}$$

Appendix B. System of 12 homogenous linear equations for cantilever T-beams

System of twelve homogeneous linear equations in twelve unknowns A_i ($i = 1, 2, \ldots, 12$):

$$A_1 + A_3 + A_5 = 0, \tag{B.1}$$

$$A_2 \frac{\alpha_1}{L_1} + A_4 \frac{\beta_1}{L_1} + A_6 \frac{\gamma_1}{L_1} = 0, \tag{B.2}$$

$$(A_1 k_{\alpha 1} + A_3 k_{\beta 1} + A_5 k_{\gamma 1}) / x_\alpha = 0, \tag{B.3}$$

$$\begin{aligned}(&-A_1 \cosh \alpha_1 - A_2 \sinh \alpha_1 - A_3 \cos \beta_1 - A_4 \sin \beta_1 - A_5 \cos \gamma_1 - A_6 \sin \gamma_1 \\ &+ A_7 + A_9 + A_{11}) \frac{1}{\lambda_{ss}} + A_8 W_{32} \bar{\alpha}_2 g_{\alpha 2} - A_{10} W_{32} \bar{\beta}_2 g_{\beta 2} - A_{12} W_{32} \bar{\gamma}_2 g_{\gamma 2} = 0,\end{aligned} \tag{B.4}$$

$$\begin{aligned}(&-A_1 \frac{\bar{\alpha}_1}{L_1} \sinh \alpha_1 - A_2 \frac{\bar{\alpha}_1}{L_1} \cosh \alpha_1 + A_3 \frac{\bar{\beta}_1}{L_1} \sin \beta_1 - A_4 \frac{\bar{\beta}_1}{L_1} \cos \beta_1 + A_5 \frac{\bar{\gamma}_1}{L_1} \sin \gamma_1 - A_6 \frac{\bar{\gamma}_1}{L_1} \cos \gamma_1 \\ &+ A_8 \frac{\bar{\alpha}_2}{L_2} + A_{10} \frac{\bar{\beta}_2}{L_2} + A_{12} \frac{\bar{\gamma}_2}{L_2}) \frac{1}{\lambda_{mm}} - A_7 W_{22} \bar{\alpha}_2 \alpha_2 + A_9 W_{22} \bar{\beta}_2 \beta_2 + A_{11} W_{22} \bar{\gamma}_2 \gamma_2 = 0,\end{aligned} \tag{B.5}$$

$$\begin{aligned}(&-A_1 k_{\alpha 1} \cosh \alpha_1 - A_2 k_{\alpha 1} \sinh \alpha_1 - A_3 k_{\beta 1} \cos \beta_1 - A_4 k_{\beta 1} \sin \beta_1 - A_5 k_{\gamma 1} \cos \gamma_1 - A_6 k_{\gamma 1} \sin \gamma_1 \\ &+ A_7 k_{\alpha 2} + A_9 k_{\beta 2} + A_{11} k_{\gamma 2}) \frac{1}{x_\alpha \lambda_{tt}} - A_8 \frac{W_{12} e_{\alpha 2} \alpha_2}{x_\alpha} - A_{10} \frac{W_{12} e_{\beta 2} \beta_2}{x_\alpha} - A_{12} \frac{W_{12} e_{\gamma 2} \gamma_2}{x_\alpha} = 0,\end{aligned} \tag{B.6}$$

$$\begin{aligned}(&A_1 W_{11} e_{\alpha 1} \sinh \alpha_1 + A_2 W_{11} e_{\alpha 1} \cosh \alpha_1 - A_3 W_{11} e_{\beta 1} \sin \beta_1 + A_4 W_{11} e_{\beta 1} \cos \beta_1 - A_5 W_{11} e_{\gamma 1} \sin \gamma_1 \\ &+ A_6 W_{11} e_{\gamma 1} \cos \gamma - A_8 W_{12} e_{\alpha 2} \alpha_2 - A_{10} W_{12} e_{\beta 2} \beta_2 - A_{12} W_{12} e_{\gamma 2} \gamma_2) / x_\alpha = 0,\end{aligned} \tag{B.7}$$

$$\begin{aligned}&- A_1 W_{21} \alpha_1 \bar{\alpha}_1 \cosh \alpha - A_2 W_{21} \alpha_1 \bar{\alpha}_1 \sinh \alpha + A_3 W_{21} \beta_1 \bar{\beta}_1 \cos \beta + A_4 W_{21} \beta_1 \bar{\beta}_1 \sin \beta \\ &+ A_5 W_{21} \gamma_1 \bar{\gamma}_1 \cos \gamma + A_6 W_{21} \gamma_1 \bar{\gamma}_1 \sin \gamma + A_7 W_{22} \alpha_2 \bar{\alpha}_2 - A_9 W_{22} \beta_2 \bar{\beta}_2 - A_{11} W_{22} \gamma_2 \bar{\gamma}_2 = 0,\end{aligned} \tag{B.8}$$

$$\begin{aligned}&A_1 W_{31} \bar{\alpha}_1 g_{\alpha 1} \sinh \alpha_1 + A_2 W_{31} \bar{\alpha}_1 g_{\alpha 1} \cosh \alpha_1 + A_3 W_{31} \bar{\beta}_1 g_{\beta 1} \sin \beta_1 - A_4 W_{31} \bar{\beta}_1 g_{\beta 1} \cos \beta_1 \\ &+ A_5 W_{31} \bar{\gamma}_1 g_{\gamma 1} \sin \gamma_1 - A_6 W_{31} \bar{\gamma}_1 g_{\gamma 1} \cos \gamma_1 - A_8 W_{32} \bar{\alpha}_2 g_{\alpha 2} + A_{10} W_{32} \bar{\beta}_2 g_{\beta 2} + A_{12} W_{32} \bar{\gamma}_2 g_{\gamma 2} = 0,\end{aligned} \tag{B.9}$$

$$\begin{aligned}&- A_7 W_{32} \bar{\alpha}_2 g_{\alpha 2} \sinh \alpha_2 - A_8 W_{32} \bar{\alpha}_2 g_{\alpha 2} \cosh \alpha_2 - A_9 W_{32} \bar{\beta}_2 g_{\beta 2} \sin \beta_2 + A_{10} W_{32} \bar{\beta}_2 g_{\beta 2} \cos \beta_2 \\ &- A_{11} W_{32} \bar{\gamma}_2 g_{\gamma 2} \sin \gamma_2 + A_{12} W_{32} \bar{\gamma}_2 g_{\gamma 2} \cos \gamma = 0,\end{aligned} \tag{B.10}$$

$$\begin{aligned}&A_7 W_{22} \alpha_2 \bar{\alpha}_2 \cosh \alpha_2 + A_8 W_{22} \alpha_2 \bar{\alpha}_2 \sinh \alpha_2 - A_9 W_{22} \beta_2 \bar{\beta}_2 \cos \beta_2 - A_{10} W_{22} \beta_2 \bar{\beta}_2 \sin \beta_2 \\ &- A_{11} W_{22} \gamma_2 \bar{\gamma}_2 \cos \gamma_2 - A_{12} W_{22} \gamma_2 \bar{\gamma}_2 \sin \gamma_2 = 0,\end{aligned} \tag{B.11}$$

$$(A_7 W_{12} e_{\alpha 2}\alpha_2 \sinh \alpha_2 + A_8 W_{12} e_{\alpha 2}\alpha_2 \cosh \alpha_2 - A_9 W_{12} e_{\beta 2}\beta_2 \sin \beta_2 + A_{10} W_{12} e_{\beta 2}\beta_2 \cos \beta_2 - A_{11} W_{12} e_{\gamma 2}\gamma_2 \sin \gamma_2 + A_{12} W_{12} e_{\gamma 2}\gamma_2 \cos \gamma_2)/x_\alpha = 0 \quad \text{(B.12)}$$

with

$$W_{11} = GJ/L_1, \quad W_{21} = EI/L_1^2, \quad W_{31} = EI/L_1^3, \quad \text{(B.13)}$$

$$W_{12} = GJ/L_2, \; W_{22} = EI/L_2^2, \quad W_{32} = EI/L_2^3. \quad \text{(B.14)}$$

References

[1] W.L. Hallauer, R.Y.L. Liu, Beam bending–torsion dynamic stiffness method for calculation of exact vibration modes, *Journal of Sound and Vibration* 85 (1982) 105–117.
[2] J.R. Banerjee, Flutter characteristics of high aspect ratio tailless aircraft, *Journal of Aircraft* 21 (1984) 733–738.
[3] J.R. Banerjee, Flutter modes of high aspect ratio tailless aircraft, *Journal of Aircraft* 25 (1988) 473–478.
[4] P.P. Friedmann, F. Straub, Application of the finite element method to rotary-wing aeroelasticity, *Journal of American Helicopter Society Annual Forum* 25 (1980) 36–44.
[5] S.P. Timoshenko, *History of Strength of Materials*, Dover, New York, 1983.
[6] V. Kolousek, Anwendung des gesetzes der virtuellen verschiebungen und des reziprozitatssatzes in der stabwerksdynamic, *Ingenieur Archiv* 12 (1941) 363–370.
[7] V. Kolousek, Berechnung der schwingenden stockwerkrahmen nach der deformationsmethode, *Der Stahlbau* 16 (1943) 5–6 and 11–13.
[8] V. Kolousek, *Dynamics in Engineering Structures*, Butterworths, London, 1973.
[9] S.P. Timoshenko, On the correction for shear of the differential equation for transverse vibrations of prismatic bars, *Philosophical Magazine* 41 (1921) 744–746.
[10] S.P. Timoshenko, On the transverse vibrations of bars of uniform cross-section, *Philosophical Magazine* 43 (1922) 125–131.
[11] F.Y. Cheng, Vibration of Timoshenko beams and frameworks, *Journal of the Structural Division—ASCE* 96 (1970) 551–571.
[12] T.M. Wang, T.A. Kinsman, Vibration of frame structures according to the Timoshenko theory, *Journal of Sound and Vibration* 14 (1971) 215–227.
[13] W.P. Howson, F.W. Williams, Natural frequencies of frames with axially loaded Timoshenko members, *Journal of Sound and Vibration* 26 (1973) 503–515.
[14] F.Y. Cheng, W.H. Tseng, Dynamic matrix of Timoshenko beam columns, *Journal of the Structural Division—ASCE* 99 (1973) 527–549.
[15] J.R. Banerjee, Coupled bending–torsional dynamic stiffness matrix for beam elements, *International Journal of Numerical Methods in Engineering* 28 (1989) 1283–1289.
[16] J.R. Banerjee, S.A. Fisher, Coupled bending–torsional dynamic stiffness matrix for axially loaded beam elements, *International Journal for Numerical Methods in Engineering* 33 (1992) 739–751.
[17] J.R. Banerjee, F.W. Williams, Coupled bending–torsional dynamic stiffness matrix for Timoshenko beam elements, *Computers & Structures* 42 (1992) 301–310.
[18] J.R. Banerjee, F.W. Williams, Coupled bending–torsional dynamic stiffness matrix for an axially loaded Timoshenko beam element, *International Journal of Solids and Structures* 31 (6) (1994) 749–762.
[19] N. Miyazaki, Application of line-spring model to dynamic stress intensity factor analysis of pre-cracked bending specimen, *Engineering Fracture Mechanics* 38 (4–5) (1991) 321–326.
[20] T. Yokoyama, M.-C. Chen, Vibration analysis of edge-cracked beams using a line-spring model, *Engineering Fracture Mechanics* 59 (1998) 403–409.
[21] T.M. Tharp, A finite element for edge-cracked beam columns, *International Journal for Numerical Methods in Engineering* 24 (1987) 1941–1950.
[22] H. Tada, P.C. Paris, G.R. Irwin, *The Stress Analysis of Cracks Handbook*, third ed., ASME Press, New York, 2000.
[23] C.A. Papadopoulos, A.D. Dimarogonas, Coupling of vibration of a cracked Timoshenko shaft, *Ingenieur Archiv* 57 (1987) 257–266.
[24] A.D. Dimarogonas, Vibration of cracked structures: a state of the art review, *Engineering Fracture Mechanics* 55 (1996) 831–857.
[25] H. Okamura, K. Watanabe, T. Takano, Applications of the compliance concept in fracture mechanics, *ASTM STP American Society for Testing and Materials* 536 (1973) 423–438.
[26] A.D. Dimarogonas, S.A. Paipetis, *Analytical Method of Rotor Dynamics*, Elsevier, London, 1983.
[27] P. Ricci, E. Viola, Stress intensity factors for cracked T-sections and dynamic behaviour for T-beams, *Engineering Fracture Mechanics* 73 (2006) 91–111.
[28] Y.Z. Chen, X.Y. Lin, R.S. Chen, Solution of torsion crack problem of an orthotropic rectangular bar by using computing compliance method, *Communications in Numerical Methods in Engineering* 13 (1997) 655–663.
[29] E. Viola, L. Nobile, L. Federici, Formulation of cracked beam element for structural analysis, *Journal of Engineering Mechanics* 128 (2002) 220–230.

[30] E. Viola, L. Federici, L. Nobile, Detection of crack location using cracked beam element method for structural analysis, *Theoretical and Applied Fracture Mechanics* 36 (2001) 23–35.
[31] E. Viola, A. Marzani, Crack effect on stability of beams under conservative and nonconservative forces, *Engineering Fracture Mechanics* 71 (2004) 699–718.
[32] J.R. Banerjee, Explicit modal analysis of an axially loaded Timoshenko beam with bending–torsion coupling, *Journal of Applied Mechanics* 67 (2000) 307–313.
[33] E.L. Shifrin, R. Ruotolo, Natural frequencies of a beam with an arbitrary number of cracks, *Journal of Sound and Vibration* 222 (3) (1999) 409–423.
[34] T.G. Chondros, A.D. Dimarogonas, J. Yao, A continuous cracked beam vibration theory, *Journal of Sound and Vibration* 215 (1) (1998) 17–34.
[35] G. Gounaris, A.D. Dimarogonas, A finite element of a cracked prismatic beam for structural analysis, *Computers & Structures* 28 (1988) 309–313.
[36] K. Wang, D.J. Inmann, C.R. Farrar, Modelling and analysis of a cracked composite cantilever beam vibrating in coupled bending and torsion, *Journal of Sound and Vibration* 284 (2005) 22–49.
[37] C. Mei, Y. Karpenko, S. Moody, D. Allen, Analytical approach to free and forced vibrations of axially loaded cracked Timoshenko beams, *Journal of Sound and Vibration* 291 (2006) 1041–1069.
[38] G. Oliveto, Dynamic stiffness and flexibility functions for axially strained Timoshenko beams, *Journal of Sound Vibration* 154 (1) (1992) 1–23.